DESIGN AND 1974 PERFORMANCE OF THE ON-LINE CANADIAN SEISMIC ARRAY MONITOR PROCESSING SYSTEM (CANSAM)

by

D.H. Weichert and M. Henger*
Seismology Division
Earth Physics Branch
Dept. Energy, Mines and Resources

Seismological Service of Canada

INTERNAL REPORT 75-13

OTTAWA

April 1975

*Permanent Address: Geological Survey of the FRG
Hannover, W. Germany

CONTENTS

1. INTRODUCTION

Following the 1958 Geneva Disarmament Conference, research and development toward detection of small seismic signals and differentiation between earthquakes and underground explosions received strong support. As a means of increasing signal-to-noise ratio, a number of seismic arrays were built during the 1960's, containing up to several hundred individual seismometers. In order to exploit the full capability of these arrays, digital computers proved to be indispensible; moreover, the large volume of data flow combined with the desirability of near-real time epicenter information required by various surveillance schemes of an envisaged treaty banning underground explosions led to an early installation of on-line digital computing systems at the large arrays. For example, when the Large Aperture Seismic Array (LASA) began operation in 1965, beamforming, detection and data editing was done by two small computers, working back-to-back for capacity and reliability (Briscoe and Fleck, 1965).

The need for the expensive on-line operation of dedicated computing systems was less acute for the contemporary medium aperture arrays, both because the data flow and storage problems were so much smaller and because the cost-benefit considerations of a relatively short delay between real-time and off-line processing at multiple-real-time speed were in favour of the latter.

The past processing mode for data from the short-period Yellowknife array (YKA) is an example of this attitude. The array was built in 1962 in collaboration between the U.K. Atomic Energy Authority and the Canadian Federal Department of Energy, Mines and Resources. Its original construction and instrumentation have been described by Manchee and Somers (1966). Briefly,

the array consists of 19 SPZ seismometers, arranged in an asymmetric cross with 2.5 km spacing between seismometer sites. From the beginning, data have been recorded in analog FM mode, and have later been digitized and processed in Ottawa. In order to establish the capabilities of the YKA and in anticipation of possible later requirements, several monitoring experiments were conducted over the years, first at double and later at four times real-time speed (Weichert et al., 1967; Manchee and Weichert, 1968; Anglin, 1971).

Two developments have now led to the installation of an on-line computer at the Yellowknife array. The first is a continuous decline of the costs of small computers, which has brought a dedicated system within the budget of a financially small organization such as ours; the other and perhaps more important development is the recognition of the valuable role YKA can play in an international network of arrays and high-sensitivity stations for the detection of small seismic events and explosions. This follows from the results of the International Seismic Month (ISM) (Lacoss et al., 1974), which was an extensive cooperative effort to establish world-wide event detection thresholds. The number of contributions by YKA to the final ISM event list was surpassed only by the contributions from LASA. Since it has been recognized that event epicenter determination using only one array is insufficient for most practical purposes, the importance of the participation of YKA and the contribution of its detection bulletin to a world-wide, high-sensitivity network becomes clear.

The CANSAM processor began operation at the end of January 1974 and it is the purpose of this paper to summarize the design of the system and to evaluate its performance to the end of 1974. More than 21,000 detections were logged during the almost 11 months of continuous operation. Most of these occurred during the summer and autumn. During the quiet season,

when Great Slave Lake is frozen, the detection system performs as predicted earlier. It is difficult to establish meaningful detection thresholds and statistics in the absence of independently determined background populations of events at the low magnitude range of interest. In our past monitoring experiments, comparison has usually be made with USGS information, LASA bulletins, etc. It is doubtful, however, that any combination of event bulletins for 1974 will ever be as exhaustive as the ISM list for February-March 1972. Instead of attempting a direct comparison, event by event, we, therefore, make extensive use of the statistical results of CANSAM test runs on ISM data, and thus establish current CANSAM capability and performance indirectly.

2. THE YELLOWKNIFE SYSTEM

2.1 The Yellowknife Array and Computer System. The physical installation of the Yellowknife array has been adequately described in the literature (Manchee and Somers, 1966; Weichert, Manchee and Whitham, 1967; Manchee and Cooper, 1968). The short-period YKA was originally constructed in 1962; in recent years a long-period tripartite array was added and the array instrumentation was updated, including the installation of a modern, two-way radio-telemetry system (Manchee and Hayman, 1972).

Figure 1 shows the location of YKA in the framework of the Canadian Seismic Network. The location was chosen, without regard to the requirements of Canadian seismicity studies, with a view towards finding a quiet intra-continental site located on the Canadian Shield and as close as possible to the Asian landmass. A compromise had obviously to be made between these desires and the ease of access and the proximity of civilization in order to attract qualified staff.

Figure 2 shows the geologic setting of YKA (Hoffman, 1969). The price paid for manageable logistics is clearly recognized here. The array is situated near the southwest boundary of the Canadian Shield, near the junction of three different provinces of the Shield. The existence of Great Slave Lake is probably due to these boundaries, e.g., the pronounced fault system of the northeast arm. In the immediate vicinity of the array, about 10 km east, we find the Yellowknife greenstone belt, an extension of the much larger area of Archean sedimentary and volcanic rocks to the east and northeast. The gold veins in this structure form the economic basis for the mines near the town of Yellowknife, an obvious source of considerable cultural seismic noise. Moreover, the geologic anomaly seems to penetrate to considerable depth and affect teleseismic signals arriving at the array from the east and northeast (Weichert and Whitham, 1969). The fine structure of the crust near Yellowknife as derived from a detailed reflection-refraction experiment has most recently been described by Clee, Barr and Berry (1974).

The geometric configuration of the array is shown in Figure 3. The short-period seismometer sites are labelled B1 to B10 and R1 to R10 with a common center point, CP. The long-period vaults are marked G1 to G3. The array centerpoint is located at 62.5^{o}N, 114.6^{o}W, the length of each line is 22.5 km, and the orientation is north-south and east-west, within 1/10 of a degree (Weichert and Manchee, 1969). The Canadian standard station, YKC, is at the location of G1. For details of the instrumentation refer to Manchee and Hayman (1972).

Figure 4 schematically shows the CANSAM computer system. Currently, it operates in parallel with the older FM recording mode, which produces 2 SP and 2 LP tapes for the Blacknest, U.K., and Ottawa research groups, respectively.

It is not planned to abandon the Ottawa SP analog tape facility, as it is considered a convenient and cheap backup data storage. The computing system is based upon a PDP11-45 general-purpose digital computer. Data enter the system from the analog telemetry channels through the signal distribution box and are multiplexed into an 11-bit bipolar analog-digital inverter. Full-scale input corresponding nominally to 500 nm/s of ground velocity is thus represented in the computer by 1023, using two's complement notation for negative numbers. Sampling rate is 20 times per second, resulting in a data rate of just over 4 kilobaud. The fixed-head disk is predominantly used as a delay line for the raw "broadband" data. In the case of detection, these data are copied to a 9-track digital tape, together with the pertinent detection parameters.

A paper copy of these detection parameters is printed on the teletypewriter, together with a paper tape backup. The daily detection log can be transferred into our Ottawa computer via a dialled telephone line. The CRT terminal is used for operator intervention, e.g., to adjust program parameters or issue calibration commands which are implemented by the computer via the serial interface.

Digitization interrupts are obtained from an internal crystal-controlled clock which is software-synchronized with an external coded timing system which, in turn, is synchronized daily with CHU.

In addition to the on-line detection log, several single-channel monitor helicorder seismograms are produced, together with a 20s-delayed record of the narrow-band detection beam. Whenever a new detection is made, this output is switched to the optimum beam, on which it then remains locked until a new detection occurs.

2.2 Beam Formation and Beam Deployment. The highly linear layout and equal spacing of the YKA short-period instruments, combined with a satisfactory uniform geological environment of all seismometer sites, lends itself to a simple and efficient method for unit-weight phased-beam formation. The method was reviewed by Weichert (1975 b) and has been in use for standard detection processing with YKA data for many years. Briefly, relative site corrections can be ignored for Yellowknife; even though deviations from great circle azimuth paths and from world-wide average travel time slopes are observed at YKA, deviations of teleseismic signals from planar wave fronts are only on the order of a few hundredths of a second. The geometrical layout is even more regular (Weichert and Manchee, 1969), so that at teleseismic frequencies around 1 Hz very little is lost by ignoring site corrections.

Beams are formed first for each line of the cross array individually by stacking the traces with delays between adjacent channels ranging from -5 to +5 digitization intervals, $\Delta t = 0.05$ s. A delay of one point, with a channel separation of 2500 m, corresponds to phasing for a slowness component of 0.020 s/km along this line. The partial beams thus obtained are then summed with the partial beams of the other line, producing a square matrix of beams evenly spaced in slowness space out to about 10 s/deg. Table I shows the beam arrangement, their azimuths and slownesses, ($dT/d\Delta$), for future reference.

Figure 5 shows the approximate location of most beams on a geographic map; distances have been calculated using Herrin travel-time derivatives for the P phase. Many beams closer than about 20° have been omitted, and positions beyond 90° are poorly defined due to the shape of the travel time derivative. The variable beam spacing reflects the non-linear relationship between the travel-time derivative and distance. Thus, the relation between beam lobe and

beam separation remains constant, i.e., the 3 db contour shown for one beam in the Atlantic shrinks for the near-distance, high-slowness beams.

Two criticisms can be raised against the use of this beam pattern: one is the apparent waste of beams in regions of no interest to explosion monitoring and in aseismic areas; the other may be insufficient beam density in regions of particular interest. Neither objection is particularly serious and could be allowed for, should this prove desirable. The time-saving from the exclusion of aseismic beams is expected to be relatively insignificant because the partial beams must be formed in any case; however, the decrease in the number of false detections, which can be expected from the omission of certain beams, appears to justify this approach in future. This will be discussed later. For the purpose of evaluating the CANSAM system and comparing it with its predecessor, it was deemed desirable to include all beams directly given by the square matrix. A demand for a higher beam density in certain areas could be derived from the experience described by Anglin (1971). He found a significant correlation between the number of detections and their estimated distance in slowness space from the nearest beam. Although part of this effect could be explained by the detection logic then used, Anglin, nevertheless, seemed to recognize the expected loss of beampower. Near the lower end of the detection frequency band, diagonally adjacent beams overlap slightly above their 3 db contour. For higher signal frequencies, the beam pattern shrinks and the loss becomes greater. For certain critical epicentral regions the detection threshold may well be lowered another m0.1 to 0.3 by increasing the beam density should this become desirable in the future.

2.3 <u>The Detection Passband and Digital Filter</u>. Although the system velocity response rolls off at 12 db per octave below 1 Hz, the strong increase

of background noise toward the usual microseismic peak between 4 and 8 s makes some additional filtering necessary for "optimum" detection. Although analog filters appear convenient and were used in the past, they would not only have increased the cost, both for filters and additional input channels to the A/D, but would have increased conversion time, memory requirements and complexity of data handling because the edited digital data on magnetic tape are required to be unfiltered. The pre-detection filter was therefore implemented digitally.

"Optimum" detection might be defined as maximum number of events detected, perhaps at a specified false alarm rate. Ideally, this would require a filter to be in some way matched to background noise, and to the number, amplitude and frequency of the event population to be detected. This was not attempted because of its complexity, especially if different types of events, e.g., explosions, are given a higher priority over low-frequency, low-magnitude earthquakes. A filter was therefore chosen by inspection, based simply on a training set of events taken from the ISM event list. Figure 6 shows the distribution in dominant signal frequency of the small magnitude events during the ISM period which were detected automatically, or could be confirmed by an analyst. Inspection of this Figure and comparison with power spectra of typical winter noise, e.g., as shown in Figure 18 below, led to the choice of the band from 1.1 Hz to 3 Hz (at -3db) for the pre-detection filter.

This filter is realized as a cascaded recursive filter with pole-zero locations as shown in Figure 7-a, and amplitude response as shown in Figure 7-b. Noteworthy may be the binary fraction in the filter constants, which improves calculation speed. The 12db roll-off due to the double zero at d.c., and 18db near 1 Hz, gives sufficient microseismic rejection. Despite the finely chosen pole locations, this filter is not visually sensitive to quantization and truncation effects down to amplitudes of about 5 units, as has

been verified with swept-frequency input signals of variable amplitude.

2.4 Detection Logic. In the past, automatic event detection for YKA was based on the so-called correlation method (e.g., Weichert et al., 1967) in which the partial beams for the two array lines were multiplied and integrated over time, i.e., smoothed or low-pass filtered. The reason for this practice was, first, the close association with the English array group who originally proposed the correlation method and used it in a special-purpose analog array data processor (Birtill and Whiteway, 1965), and, second, the results of Manchee and Somers (1965) who showed that this method had a slightly sharper response than other methods tested. This method of detection processing has now been abandoned since its small gain in directivity does not seem to warrant the extra expense in calculation time, and other small disadvantages.

Similar to practice at other arrays, the beams are now rectified and passed through two low-pass recursive filters corresponding to averaging lengths of 1.6 s and 25.6 s, designated STA and LTA respectively. A detection is declared whenever the STA of a beam exceeds its LTA by a preset ratio, 2.25 during 1974. The only real difference from systems used elsewhere may be the lack of a significant additional delay of the LTA: this tends to discriminate slightly against very slowly emerging signals, since such a signal immediately begins to raise the LTA. Similar to the arbitrary setting of the lower frequency corner of the detection filter, this logic tends to discriminate in favour of impulsive (explosion-like) events.

The detection logic is currently entered every 0.8 s, i.e., twice per STA averaging length which is considered an adequate overlap, except for arrival time determination: here the contribution to the root-mean-square

timing error due to this quantization is expected to be on the order of 1/6 s.

When the STA rises above the threshold, long-time averaging is suspended. Declaration of detection status is still delayed until the beam passes through its next maximum: this improves the estimate of event magnitude and, even more so, of its slowness and azimuth of arrival. The reported arrival time, however, corresponds to the first passage of the STA through a threshold somewhat below the detection threshold.

When a detection has occurred, the parameters are logged on the teletype and magnetic tape; all single-channel broadband data are copied from the disk to the magnetic tape, and the helicorder output is switched to the new beam. Figure 8 shows the 1974 format of the detection log. Most entries are self-explanatory; the beam number can be interpreted as an approximate epicentre region for teleseismic P-phases by using Figure 5 or Table I. The entry currently marked LOG A/T is a misnomer: it is actually the STA, which is a measure of the integrated signal, i.e., ground displacement. Since no estimate of signal frequency is currently obtained, the STA is, on purpose, not directly expressed in terms of event magnitude or ground velocity. However, a semi-empirical calibration of LOG A/T will be given in a later section. Background noise on the detection beams is simply the LTA of that beam.

During 1974, trigger status was terminated after at least 40 s, i.e., 20 s of pre-event noise and a minimum of 20 s of event data are saved on digital tape. After this minimum time, trigger status is maintained until the STA sinks below its pre-event LTA. Improving these switch-off criteria is not considered very important, unless masking of subsequent events appears to become problematic. During the 11 months of operation in 1974, an edited

digital event library of 71 2400-ft. tapes was created. Following a second, off-line editing process, most of these tapes will be recycled by 1976.

2.5 Log-Sum Processing. In the past, seismic array data processing has predominantly utilized linear methods, such as straight summation, delay-and-sum, or weighted delay-and-sum. More complicated, yet still linear processes are maximum-likelihood and Wiener processing. A good comparison of these methods was given by Green, Kelly and Levin (1966). The approach normally starts from the desire to maximize signal-to-noise ratio with a minimal distortion of the signal waveform. For detection processing, the distortion requirement is not very important, and it appears that significant gains can be made if it is sacrificed.

For instance, Melton and Karr (1957) showed from basic probability theory that a simple sign-coincidence scheme would improve the probability of detection of a coherent multichannel signal. In essence, the method consists of summation of all channels after clipping the signal to ±1. Less drastic non-linear signal transformations have been championed by Muirhead, using Warramunga seismic array data (1968) and by Kanasewich et al. (1973), who have both shown good signal-to-noise ratio gains with n-th root processing. Extracting the n-th root from the single channel signals before phasing and adding again decreases the weight of single-channel amplitudes and thus emphasizes signal coherence.

Weichert (1975a) has described a computationally more attractive method, which has been incorporated as an option into the CANSAM detection processing system.

Each channel, represented by x, with $|x| = 2^n \cdot f$, $1 \leq f < 2$, is transformed according to

$$y = \text{sign}(x)\ (n + f - 1) \times 16$$

The bracketed term on the right is an approximation to the binary logarithm of x, in fact so close that over the full scale input range the difference is barely visible to the eye. The process has been named "log sum processing".

It should be well understood that this is an ad hoc procedure; experimenting with it in an on-line detection mode was justified by the previous success of Muirhead, supported by the limited theory of Melton and Karr. Extensive comparison with the linear summation method as described below has provided convincing evidence of its superiority, and the log summing option was therefore used in the CANSAM detector throughout 1974. Continued use, however, will be accompanied by efforts to tie the background noise distribution into the theory of optimum detectors, relaxing the requirements of signal fidelity, perhaps along the lines suggested by Capon (1961).

2.6 CANSAM Test Runs on ISM Data. The event data list compiled by Lacoss et al. (1974) afforded a unique opportunity to compare the CANSAM system detection capability to a known event population. As already pointed out above, the YKA contributions to this event list were second in number only to LASA detections. This was achieved with the older processing system, using analog recordings of the YKA data. The first test for CANSAM consisted in rerunning these data and a comparison of the two sets of results. It was found that CANSAM automatically detected essentially the same events found with the earlier processing system, plus the events that had only been verified by the analyst by special processing on hind-sight. No special attention was paid in this comparison to the number of false alarms in each system, except that the false alarm rate was low enough to avoid any noticeable

windowing or blocking effect, which would result from the restriction on the detector to ignore new energy arrivals while in detection status.

A second, more significant comparison experiment tested the difference between the linear-sum and the log-sum detectors. Detailed results are described in a separate paper (Weichert, 1975a). Briefly, during the 390-hour test period, the log sum detector detected about twice as many ISM-verified events as the linear detector for a given false alarm rate or, alternatively, for a specified threshold magnitude, the linear detector had a 5 times higher false alarm rate than the log detector. False alarms, in this context, were simply defined to be all detections not verified by the ISM event list.

Specific identified types of false alarms which were known to plague the linear processor, but which the log process suppresses very successfully, are:

- non-planar surface waves from nearby mine explosions. These signals have periods of almost 1 s, and occasionally are misinterpreted as teleseisms by the station operator on single channel monitor records.
- ice-noise (ice quakes) off Great Slave Lake during winter periods of large temperature variations.
- maintenance work or calibration signals on single channels. This type of false alarm could obviously be suppressed by additional programming, i.e., exclusion of such channels from beam forming; however, this is not necessary with the log detector and, in any case, this suppression provides excellent evidence for the emphasis on signal coherence over single-channel amplitude, ascribed to the log sum process.

The results of the comparison are shown in Figure 9. The cumulative number of events, essentially the same in both runs, are plotted

against the log beam amplitude; they exhibit a slope of about -0.8 per unit magnitude, which is within the generally accepted range of the event number-magnitude relation. Here, the equivalent YKA magnitude has been obtained by a semi-empirical calibration against ISM-given magnitudes, similar to the calibration to be reported below for 1974. The shoulder of the linear-detection false-alarm-rate curve was caused by single-channel calibrations. After their removal, the modified linear-detector false-alarm line becomes closely parallel to the log-detector false alarms, but remains about 0.3 magnitude unit to the right of the comparative line.

Figure 10 shows examples of the beam seismogram obtained with the two processes. In general, it appears that the logarithmic beam results in a more pleasing, though less familiar, seismogram. The Honshu event at m_b5.7 nearly saturates YKA. The linear beam trace shown in the upper portion of the Figure clutters the seismogram, fades badly, and its maximum amplitudes are barely visible. The log beam trace of this event is strong, and every energy burst can be seen at least as well as on the linear trace. On the other end of the magnitude scale, what is believed to be the Fox Island event of m_b3.6 at 21:46, appears similar on both seismograms. This is expected since at low amplitudes the logarithmic transformation is almost linear. The spiky event, near 21:17 on the linear seismogram appears to be a misphased local event which the log-detector suppresses. Finally, the m_b3.9 Turkey event in the lower left corner was not detected by the linear-sum detector.

3. EVALUATION OF 1974 ON-LINE CANSAM PERFORMANCE

The CANSAM computing system was installed in Yellowknife early in 1974 and first began operation on 28 January 1974. Hardware and program

modifications continued until 8 February. The period evaluated in this paper begins at that date and ends at the end of 1974. However, performance monitoring continues, and no significant deviation from the 1974 system behaviour is observed; the results described below can therefore safely be extrapolated. Program and parameter changes which appear desirable from the present study were implemented in April 1975.

The larger study, of which this paper is the first part, serves two purposes: foremost, it is to define and document the contributions which the YKA array can make in its new on-line operation on a year-round basis to a world-wide network of high-sensitivity stations for detection and location of low-level seismic events. Secondly, it is to form the basis for a decision to curtail or close down the operation of the present Canadian standard station, YKC, which is located near the array. For this purpose the array and its associated recording and processing system must not only match the high standard of reliability of the standard station in terms of operational status, easy availability of standard seismograms, either in the form of continuous monitor records or special playbacks, but it must also match or exceed the standard station event lists and arrival time accuracy. For teleseismic events, there is, of course, no problem, but for regional (Canadian) seismicity the present array processing system may not be sufficiently optimized. 1974 Canadian seismicity as observed by CANSAM will, therefore, form the subject of a later special study and only a preliminary comparison with reported regional event lists is included in this first paper.

3.1 System Reliability. Generally, increasing complexity increases the probability of failure of one of its components. For the purpose of this study we have considered the CANSAM system to be operational as long as a detection

log and monitor record was produced. Failures of other important components can often be tolerated. For instance, breakdown of either the disk or the magnetic tape drive will eliminate the edited digital event tape. This is not considered very serious at the present time, because the analog recording backup still exists and has a very high reliability. Digital tapes could therefore be produced on demand within a short time. On the other hand, maintenance or repair work on these peripherals will usually result in a shutdown of the whole CANSAM system. The following statistics are to be understood within these constraints.

The downtime from 8 February 1974 to the end of the year was 7.9%, of which only about one-half has been identified by causes. Table II lists the major causes and the resulting time losses.

Power problems have been the dominant cause of malfunctions. Fluctuations of both voltage and frequency often stray outside the computer specification. It is suspected that disk problems were caused by these deviations. Improvements have been made, resulting in better performance during the latter months of the year, but fully adequate power regulation and backup are not yet planned.

Power variations affect all seismic channels simultaneously: as a consequence, the background noise level of the unphased partial beams in the detection beam matrix is always higher than on other beams, even in the relatively high-frequency predetection passband. As a result, the zero-delay beam 74 (c.f. Table I) had to be inhibited in the trigger logic early in the year, since it gave an intolerable number of triggers, well correlated with time of the day (e.g., shift changes in the nearby mines).

Initially, the powerfail/upstart interrupt service provided in the

computer program did not function properly, so that additional unnecessary downtime was incurred after nighttime power failures. Moreover, the digital tape deck must still be restarted manually after a power failure, resulting in additional losses of digital event tape.

Figure 14-b shows the time percentage of operational status of the detection system throughout the year, averaged over 7-day periods. The low at the end of March is mainly due to operator training and program changes connected with improving automatic arrival time. The low in April-May was due to disk failures. Power failures during June-August may be related to thunderstorm activity, and the low percentage at the end of the year was caused by a tape deck failure.

3.2 Quality of Automatic Event Arrival Times. To check the consistency of event arrival times obtained automatically, the arrival times of 967 events were compared with the times read and reported by the operator of the standard station, YKC, which is located 6.5 km at an azimuth of 106° from the array center point. The period chosen for this comparison was April to December only, since before April the timing logic of event onsets was changed several times. Corrections for the location difference have been applied.

Monthly histograms of the timing difference YKC (operator picked) - YKA (automatic) were plotted (not shown). A common feature is a small negative offset of the average. Moreover, during the summer months there are not only fewer common events, but the scatter of the timing differences increases. This is obviously due to the increase in background noise level during the summer which increases the detection threshold and makes reading of onset times less reliable. It therefore appeared desirable to group arrival time estimates seasonally in a fashion similar to other event statistics to be

discussed later.

Figure 11-a and -b show the combined histograms for 1 June to 30 November and for April-May and December. It is noted that in both seasons the computer sees events slightly but significantly earlier, on the average, than the operator. Although time differences greater than 4 s were ignored in this calculation, the average is obviously biassed towards "YKA early" due to the large numbers of late operator readings near 1 s and more. The median in both seasons is close to zero, or insignificantly negative, i.e., YKA late. A late reading of 0.4 s average would be expected because during 1974 the trigger routine was entered only every 0.8 s and the computer could see the upbreak only after it occurred.

Contribution to the variance of the difference in arrival time comes from three sources: scatter in operator and in computer timing and the time quantization effect of the detection logic. The latter contribution is estimated as $(0.23\ s)^2$. This is considerably less than the actually observed variance of about $(1\ s)^2$, and we conclude that at the present time the dominant contribution to the timing scatter comes from either the operator or the machine arrival times.

The restriction on the trigger logic during 1974 resulted from consideration of computing time. Since some planned program extensions have been cancelled, the trigger logic is entered every sampling interval (0.05 s).

3.3 Missed Events. Despite the undoubtedly high capabilities of the array processing system, not all phase readings reported by the operator of the standard station have been automatically detected. This is statistically to be expected and is hardly significant, but becomes serious when closure of the standard YKC operation is considered. CANSAM has been designed primarily for detection of teleseismic events with their characteristic range of frequencies, slownesses and good coherence across the array. We first checked the standard station teleseismic phase report sheets and tried to identify the reasons for any events missed by CANSAM. Table III shows a breakdown by months of the number of operator-reported presumed teleseisms, the number missed by CANSAM and the number missed while CANSAM was actually operational.

The percentage of events missed due to system downtime corresponds closely to expectations: 9.3% against 7.9% of downtime actually identified. The difference may well be significant, as the longest periods of inoperational time occurred during the quiet season when the number of operator-reported events was high, as illustrated by Figure 12-b and -c.

Other causes for non-detection could be specifically identified in many cases, but there is no dominant cause and the approximately 2% miss-rate, which appears rather stable from April onward, is unlikely to be decreased easily. Some events had dominant periods well above the CANSAM detection band and the loss of these events was anticipated. Similarly, we expected to lose some events during the detection status resulting from a previous event or noise detection. The probability for this to happen increases as the detection threshold is lowered, and it becomes appreciable during the high-noise summer months. In a few other cases, no evidence for an event could be detected by three independent trained analysts, but this does not

include events where the operator had made obvious timing errors of 15 minutes, or similar errors. At least one missed event was reported by YKC as a teleseism, but turned out to be a 1-s surface wave pulse diverging from one of the local gold mines (c.f., also Sect. 2.5, log-sum processing).

For local, or better "regional" seismic events, the miss-rate is expected to be higher, since the slowness of these signals can be well above 100 ms/km, their frequencies are higher, resulting in sharper main lobes of the beam, and, finally, the coherence of the signal front across the array is not as good as for teleseisms. A detailed study of the usefulness of CANSAM for investigations of Canadian seismicity will be the subject of a future paper; here, we restrict ourselves to the following comparative tabulation (Table IV).

The number of events missed due to CANSAM downtime is again near the average downtime. The reason for separate consideration of "high quality" events is the instruction given to station operators to include all possible local readings on the report sheet. "High quality" events are defined as events for which the operator was able to read an amplitude and/or an S-P time; thus many locals, or regionals, are no more than wiggles on a single array channel, and not necessarily visible on the 3-component standard station records.

3.4 Amplitude-Magnitude Calibrations. In much of the following we will refer to 1974 statistics in terms of the logbeam amplitude. Although it is relatively simple to relate the amplitude of the phased logarithmic sum, as displayed on the monitor helicorder, directly to average ground velocity, no such simple relation holds for the rectified and pseudo-exponentially smoothed beam as used in the detector. Even if such a theoretical relationship could be more reliably given, the final judgement of the CANSAM threshold would necessarily be based on a comparison with an external reference event population, with

all its inherent uncertainties and magnitude scatter. We therefore present here only extremely simplified relations between the logarithmic-beam amplitude and the average ground velocity,
then proceed directly to a comparative calibration against USGS magnitudes for 1974 and ISM magnitudes for the 1972 one-month period.

The logarithmic transformation of the single-channel signal yields 16 quantum units (qu) for 1 qu input, corresponding nominally to 0.5 nm/s ground velocity, and 16 qu for every factor of two. The predetection filter has an average gain in the passband of about 1.5 . Assuming identical signals on all 19 channels and taking into account the scaling internal to the computer and output sensitivity of 1 V/cm, one obtains for ±1 nm/s input a helicorder amplitude of

$$H = \frac{\pm 32 \cdot 1.5 \cdot 19 \cdot 5 \cdot 10 \text{ mm}}{2 \cdot 16 \cdot 2048} = \pm 0.7 \text{ mm} \quad .$$

Maximum ground velocity of ±500 nm/s similarly leads to about ±3.85 mm on the monitor seismogram. This relation, holding for perfectly correlating signals, is shown in Figure 12. The auxiliary magnitude scale is arbitrarily based on 1 nm/s = m3.0, corresponding to a distance correction function of Q = 3.8, a convenient third zone average. As expected, the observed PDE magnitudes cluster along a line somewhere between the line for fully coherent signals and the line for incoherent signals. This is due, of course, partly to incomplete coherence, partly it may reflect a station magnitude correction for YKA and, thirdly it may be due to a positive network bias of USGS at low magnitudes, as would be suggested by the distinct separation of USGS and ISM events in the low magnitude range of Figure 13.

A similar semi-qualitative analysis of the log beam must, in addition, take into account the averaging of the rectified sum. The z transform

of the recursive low pass filter used is $(1-31z/32)^{-1}$, giving a gain of 32 for the d.c. of the rectified waveform, and approximately -20db in the pre-detection passband. However, for the transient character of seismic signals, the time domain description of this filter may be more relevant: it is a running average over a (pseudo) exponential window with a width equivalent to 32 points, i.e., 1.6s, of a square window. Thus, the actual response depends very much on the waveshape and length being averaged, or integrated, and no easy relation between logbeam amplitude and ground displacement can be given. In view of these uncertainties, we proceed immediately to a direct calibration of the logbeam against magnitude.

Figure 13 shows USGS PDE magnitudes plotted against logbeam magnitudes as given in the CANSAM detection log. The events were randomly selected from the 1974 PDE cards; they do not represent any particular period during 1974, nor a selected geographic region, except that the events occurred in the third zone from YKA. Also shown are events from the ISM list, in order to give more data at low magnitudes.

We conclude that the scatter of observed points is completely consistent with the scatter usually observed in magnitude comparisons between single stations or networks, and there exists no inconsistency between the different methods of establishing the relation between bits in the computer and event magnitude. At the lower magnitude end, PDE magnitudes are distinctly higher than ISM: this may be due to a bias introduced by the diminishing number of stations still detecting these small events, or uncertainties in the distance correction function. The linear relation between logbeam and m_b obtained from the calibration plot in Figure 13 is shown as an auxiliary scale on many of the subsequent plots.

3.5 Detection Thresholds and Noise Background. In the past, the detection threshold of the Yellowknife array has variably been expressed as 50% or 90% cumulative, or occasionally incremental, detection of events which could be verified and their magnitude obtained from an independent event list. See, for instance, Weichert et al. (1967), Manchee and Weichert (1968), Anglin (1971). In an earlier section (2.6), the threshold magnitude was similarly determined by comparison with the ISM event list, but for the first time a definite relation between threshold and false alarm rate was given. It was shown that the cumulative event population fitted a straight line with slope near -0.8 on a plot of log N against the logbeam amplitude, while the false alarm population had a slope of about -3. Lacking a convenient small-event background, we shall utilize these results to define event and false alarm populations during 1974.

In Figure 14 we have summarized the seasonal variation of several relevant detection statistics. Plotted against day of the year, (a) shows the variation of the weekly average noise background on those beams on which detections occurred. The noise samples were taken as the LTA's at the time of detections: the sampling, therefore, cannot be considered random in amplitude. Especially during the noisy season, the averages may be biassed towards high values. This follows from the frequently observed slow emergence of typical false alarms, which would tend to pull the LTA up before a trigger occurs.

Regardless of such bias, the noise exhibits a clear semiannual variation, a quiet and stable winter condition and a noisy and more variable summer background. Investigations to be described below clearly identify Great Slave Lake as the source of the summer noise. Inspection of 1974 satellite

photos revealed a close correlation between background noise and the presence of ice cover on the lake. Early in May, the first ice breaks could be discerned, but complete disappearance of the ice cover was not observed before mid-June. Because the satellite covers the same line only every 5 days, and only 2 adjacent lines show enough of Great Slave Lake to judge the overall state of the ice, the schematic breakup shown in Figure 14 must not be interpreted too literally. Similar uncertainties were encountered in observing the winter freeze-up. In the second half of October, ice had formed in the N-W arm, and its advance could be followed towards the main body of the lake. However, since the satellite passage occurs in the morning, the lengthening winter nights prevented observation of complete freeze-up. The schematic for this time simply reflects this uncertainty and is drawn to fit the decrease in noise level.

Figure 14-b and -c have been introduced earlier; -c shows weekly averages of the number of daily detections. The large variations during the spring are partly connected to processing system failures, as discussed earlier, but probably also reflect short-term fluctuations in seismicity; for instance, the peak in early May correlated well with the increase in -d, the number of events reported by the standard station operator. Peaks during summer months seem to correlate with the background noise and are expected to be predominantly false alarms. No explanation can be offered for the stable detection level during October and November, during which time the noise background already declined steadily.

On the basis of the summary statistics in Figure 14, it was decided to define the noisy or summer season as the 6-month period from 1 June to 30 November, the remainder of the year as the quiet or winter season, and to

present the following more detailed statistics separately for these two periods.

Cumulative daily averages of the LTA are plotted in Figure 15-a (left hand percentage scale). For later reference, it should be noted that at the 10% level of occurrence the background noise in summer and winter is separated only by the equivalent of m0.2. As above, we note that daily averages may be biassed towards high values, especially during the summer season, which would tend to accentuate the difference between the seasons.

Figure 15-b shows the cumulative numbers of detection for the two seasons. During the winter, we observe a striking similarity with the corresponding graphs for the ISM test experiment, Figure 9. One obvious difference is, of course, the absolute number of detections during the two periods, 16 days in Figure 9, while Figure 15 represents about 150 days, but has been normalized to half a year for the winter season. Second, the log detector during the ISM experimental run was set at a slightly lower signal-to-noise ratio than in 1974, resulting in a cut-off near 4000 qu instead of about 6000 qu (m4.0).

Third, Figure 9 shows a verified event population separate from "false alarms", which includes all unverified detections, while the data in Figure 15 are total detection numbers.

We note that both seasonal detection curves in Figure 15 can be reasonably well approximated by two straight lines each, with short transition curves. The slope of the winter line near the high-magnitude end matches the slope of the corresponding ISM event population closely. It can be concluded that it represents the 1974 winter event population. Moreover, it corresponds closely to the well-known $\lg(N)-m_b$ relation.

Although at low beam amplitudes the winter-season cumulative plot

clearly bends up, the slope does not become as steep as the corresponding segment for the summer season, nor as steep as the false alarm line in Figure 9. Since the latter two lines agree closely in slope, it can be concluded that the upper part of the summer line in Figure 15 is dominated by noise detections as well, but the upper portion of the winter curve has not fully turned over and is a mixture of comparable numbers of seismic events and false alarms.

To obtain a realistic comparison of the quiet-season curve with ISM results, we extend the straight event line up to the left, subtract the number of events thus obtained from the total number of detections and finally draw a false alarm line through the points thus obtained. The slope of this line is almost identical to the other two false alarm lines, which gives additional justification for the procedure. The 50% false alarm rate defined by this indirect method is near 6800 qu, about m4.0, which is definitely lower than in the ISM experiment (7400). This was expected for two reasons: first, because the ISM false alarm population was thought to contain a significant number of non-verifiable events and, second, because the on-line CANSAM eliminates the additional noise connected with the intermediate analog FM data recording. The crossover of the false alarm and event lines just about coincides with the detection cut-off: this is not an accident, since the detection SNR was set for a 50% false alarm rate on the basis of the off-line simulation.

Interpretation of the summer-season curve presents ambiguities. First, the event slope is slightly steeper. This would be partly caused by contamination from the false alarm population and could be allowed for. Rounding at the cut-off of the curve at low magnitudes is more pronounced and, finally,

the actual cumulative numbers at the right end of the summer event line become rather small, so that elaborate analysis of the summer detection curve does not appear to be justified. We simply estimate the approximate position of the summer false alarm line, as indicated by the cross-hatched area below the summer detection curve. The lower limit is constructed from the uncorrected event line as shown and reflects its slightly steeper slope; the upper limit is based on an event slope equal to the winter slope and passing through the right end of the summer event line. The upper end of the shaded area is poorly determined because of the broad, rounded upper shoulder of the summer detection curve: the cause for this is obviously the broader range of variation of the background noise and the fixed signal-to-noise ratio of the detector.

Important conclusions to be drawn from the data in Figure 15 are the following. During the winter half year, from 1 December to 30 May, the detection threshold as defined by a 50% false alarm rate is at m4.0, giving about 30 detections per day. Small improvements can still be expected from program parameter changes to be discussed later. During the summer half year 1974, a similarly defined threshold was closer to m4.8. Changes of program parameters during the summer months are expected to improve this threshold significantly, perhaps to m4.4-4.6.

The number of noise detections during the summer is so much greater than would be expected from the variation in background noise alone, considering the constant signal-to-noise threshold setting of the detector, so that a significantly different noise source and distribution must be assumed for the summer months. We have already correlated the seasonal difference qualitatively with the existence of ice or open water on Great Slave Lake. A

more detailed investigation of the summer noise will be described in the next section.

The over 16000 detections during the summer half-year pose another problem. Because each detection status lasts for a minimum of 40s during which detection of other events is inhibited, the probability of missing events because of noise triggers may begin to become appreciable. However, in order to explain the lower level of the summer event line, about a factor of two lower, one would have to assume that the 16000 detections block about one-half of the total time. This would require an average of about 7 minutes for each period of detection status. This average has not been calculated, but appears unlikely, and thus the discrepancy in numbers of events during the two seasons is unresolved. The cumulative numbers appear to be too high to suggest a real variation of numbers of seismic events within detection range of YKA. An investigation into such a real annual variation on the basis of outside event bulletins would have to take into account a possible seasonal variation of detection capability of the contributing stations at the lower magnitude and would, therefore, not be as straightforward as one would hope.

4. THE SUMMER NOISE PROBLEM.

During the past years, continuous processing experiments with YKA data were restricted to the early months of the year and results have been published with the caveat "during the quiet season of the year". The major reason for avoiding automatic detection experiments during the summer was, however, not so much the higher seismic noise level during this part of the year, but the much higher rate of equipment failures due to thunderstorm-

induced transients in the early years and, in 1972, the timing of the International Seismic Month, which again fell into the YKA winter season. It is, therefore, only now that we are really faced with the serious problem of high false alarm rates during the summer. Because the detection threshold floats a factor of $2\frac{1}{4}$ above the background noise, one would expect the false alarm rate to remain essentially constant if the distribution of the noise remained the same. This is obviously a fallacious assumption. Three aspects of the summer noise were consequently studied in an attempt better to understand the reason for the false alarms and to find ways of suppressing it. First, the unfiltered, single-channel data were examined in detail for many of the detections throughout June to November. Second, the distribution of detections in slowness space, both for winter and summer condition, was investigated and, finally, the variation of noise power spectra between winter and summer conditions was studied.

4.1 Time Domain Study of False Alarms. A number of low-amplitude detections were selected from the YKA bulletin according to the single criterion, that they did not appear to be teleseismic events to the eye of a trained analyst. Table V lists in the first 5 columns the relevant detection parameters taken from the detection log. The log A/T column shows the beam amplitude and gives an idea of the approximate equivalent magnitude (c.f., Figure 13): all detections have an apparent magnitude near m4.5.

None of these events shows a distinct beginning. Typically, they have a sinusoidal appearance with a visual frequency just above 1 Hz and build up gradually from an always present background of similar frequency. Correlation between array sites is sometimes difficult, particularly along the east-west line. Figure 16-a shows as an example the detection window at 74 Jun 23 0713Z. Also shown is an attempt by

the analyst to line up what appear to be corresponding waveforms. The seismic traces joined by a line on the left are the north-south array line, south being left; the next 9 traces are the east-west array line, east being on the right end. The dashed kink between channels 18 and 19 indicates that the array center-point trace, common to both lines, (channel 6) has not been repeated at this position. A least squares fit of a linear wavefront intercept with the earth's surface gives an azimuth of 146° and a slowness of 0.364 s/km, as shown in the Figure. Least squares fits for the other detections in Table V have been made and the results are shown in that Table. Despite the small standard deviation shown in the sample figure, the actual variations in azimuth and slowness for the different samples are not very significant, considering the difficulties of correlating the signal across the array, especially along the east-west line. The formal standard deviations given by the computer probably include the result of prejudging, prefiltering or smoothing the time picks on the display screen by the analyst's eye. No attempt was made to analyse long-term variations of arrival azimuth (or slowness) of the noise detections, but a qualitative correlation between wind at the array and noise level was looked for: although many high-noise situations coincided with high winds, several others did not. To prove a cause-effect relationship, other considerations would have to be taken into account. For instance, available wind speeds were non-directional early morning estimates on land near the control center and do not necessarily reflect the probably more geostrophic winds over open water near the 100-200 km distant lake areas which would be the source areas for the observed noise.

The right-most trace in Figure 16 is the sum of all array channels. Only a small amplitude is observed in -a. In Figure 16-b, the channels have

been delayed for an arrival azimuth of 150° and a slowness of 0.3 s/km. Trace 21 now gives appreciable power and the line-up with these parameters appears very good. The same observation is made for all other investigated detections in Table V and we conclude that the predominant summer noise at YKA is an approximately 1.2 Hz surface wave propagating with about 3.0 km/sec, and an almost linear wavefront from the direction of the center of Great Slave Lake, at about 150° azimuth.

If we multiply this average velocity by $1.1*\sqrt{3}$ to obtain an estimate of the corresponding P-wave velocity, we obtain 5.7 km/s, which is the P_g velocity ascribed to a granitic surficial layer of about 1 km thickness by Barr (1971), Weichert (1969) and by Clee et al. (1974); this indicates that our dominant summer noise may be a guided Rayleigh wave in this upper layer, existing uniformly in the array area west of the Yellowknife Greenstone Belt, and excited by wave action on the lake.

Figure 16-c shows a trace alignment corresponding to the beam on which this detection occurred. Again, appreciable power is obtained on trace 21, the array sum. It should be pointed out that the proper phasing for this surface wave cannot be included in the set of beams formed on-line by the computer, because of memory limitations due to the long delays. Even the major sidelobes for the particular detection in Figure 16 are outside the usual beam matrix, but it can be shown that the actual detection beam is close to a major sidelobe and probably corresponds to a minor sidelobe.

4.2 Distribution of Noise Detections in Slowness Space. To illustrate in more detail the question of sidelobe triggering and what to do about it, the cumulative detection numbers on each of the 121 beams were plotted against the log beam amplitude, similar to the cumulative distributions shown in

Figure 15-b. These distribution curves are again separately calculated for the winter and summer seasons and are presented as a matrix in Figure 17-a and -b. Seismic beams are easily recognized in the winter season (-a) by two criteria: the number of detections is significantly higher (c.f., number and log-amplitude scales in lower left corner) and the change of slope between log-beam amplitude ranges dominated by seismic events and noise triggers, respectively, is clearly evident on these beams. A separation of the two populations for each beam, as was done in Figure 16, was not attempted because the small numbers cast doubt on the significance of the results. However, for beams covering certain epicentral areas, such separation may still lead to useful results. For similar reasons, it does not appear useful to discuss the significance of differences in slope (the constant b) of the cumulative event lines on different beams.

It is clear from Figure 17-a that during the winter season the false alarm rate could be decreased from the 1974 rates without great loss of teleseismic detections, either by inhibiting detections on the non-seismic beams or by increasing the thresholds on them significantly.

For the summer season, Figure 17-b, the outlook is not as optimistic. Several seismic beams have become almost irrecognizable; the transition of the steep false alarm line to a flatter seismic-event line has disappeared in many cases, but the number of total detections, obviously false alarms, has increased immensely on a broad east-west band of slowness with a small northerly component. This seems to indicate that we do not trigger on one particular sidelobe of the surface wave from Great Slave Lake. Consideration of the array response shows that no major sidelobes of these signals are covered by the CANSAM beam pattern, but, depending on signal frequency, one major lobe falls E-NE of

the beam matrix and a row of secondary maxima passes through the northern half of the beam pattern. Detections are therefore governed almost by chance, depending on the exact, but slightly variable, relation between beams and sidelobe position. This explains qualitatively the east-west trending band of increased noise detections.

Reduction of the false alarm rate appears difficult. The surface wave frequency, about 1.2 Hz, falls into the detection band. Steering of a zero beam response towards the noise regions does not help, because it will be aliassed into the region of interest as well. A relatively small reduction can be achieved by inhibiting non-seismic beams, a correspondingly larger reduction by concentrating only on a few certain beams. Finally, the detection pass band could be narrowed with a sufficiently steep flank towards the noise. If the real-time operation of the array becomes dedicated to explosion detection, perhaps a combination of these methods will be the most effective solution.

4.3 Noise Spectra. We have already unambiguously identified the source of the high-power, 1 Hz noise signal and now wish to present a study of the distribution and variation of this noise power in the frequency domain. For this purpose, we selected 10 background noise periods of 12.8 s each, both during a quiet day in April and during an October day, selected visually from monitor records for its high noise level. The dates and times of the noise samples are shown in Table VI. After windowing the samples with a squared-sine function over 12.5% of their length at each end, power spectra were calculated with a standard Fast Fourier transform program. The 10 power spectra for each day were averaged to obtain more stable single-channel spectra representative of the quietest and noisiest conditions.

In Figure 18-a and -b we show these spectra for each period. No correction for seismometer response has been applied (-12 db/octave below 1 Hz). The 90% confidence interval of about 6.6 db for 10 degrees of freedom is indicated in the Figure. The significant difference between the two seasons is the presence of the broad, high-power peak near 1 Hz, which does not exist during the winter season except on the most southerly array sites near the shore of Great Slave Lake. Less significant is the increase in power in the usual microseismic peak from April to October by an average factor of 5, with a small shift of its peak frequency from about 0.3 Hz to below 0.2 Hz. This increase in microseismic power seems more pronounced near the shore at the south end of the array.

For purposes of event detection the normal microseismic peak is of little concern, because the predetection digital filter gives an additional 12 to 18 db in this frequency range, which approximately matches or exceeds the flank of the microseismic peak.

The broad summer peak near 1 Hz, however, is a very serious drawback for detection of small events. Its maximum occurs at a slightly variable frequency, from about 0.8 Hz to 1.1 Hz, with a slope of -18 db out to about 3 Hz. At the low frequency end, this peak continues up to the 5 s microseismic peak, but in all spectra it can be recognized at least as a well-defined shoulder on the flank of the microseismic peak. The major contribution of the 1 Hz microseismic peak occurs approximately in the band from 0.43 Hz to 1.29 Hz: an integration over this band leads to an average rms noise of 4 nm/s for the April samples and 28 nm/s for October. This should be compared to the results of Burch (1966), who studied noise background at several medium aperture arrays, including YKA. He used analog methods and quoted equivalent sinusoidal zero-to-peak voltages for several octaves: for the 0.5 Hz to 1.0 Hz band, his

results are equivalent to 3 and 20 nm/s rms for his quietest and noisiest periods, respectively. This is marginally lower than our calculations, but his bandwidth is also narrower. Moreover, the measurement must be very sensitive to the cut-off at the low frequency end, where the contribution from the 5s microseismic peak becomes quite appreciable. Burch noted the high 1 Hz power, but did not recognize its origin.

Attenuation of the power in the 0.43 - 1.29 Hz band away from Great Slave Lake is shown in Figure 19. It shows the integrated power, plotted as a function of site distance from the center of Great Slave Lake, i.e., the sites are projected onto a line bearing S30^{o}E. It was demonstrated earlier that these waves generally propagate from this direction with a velocity of 3.3 km/s. Although there are exceptions, the trend of decreasing power towards the NW appears quite significant. The high noise level near the western end of the array could be explained by the close distance of these sites to the actual shoreline, which curves around the array in a sweeping arc, forming the northern shore of the N-W arm of the lake. Because of the anomalous power levels near the ends, a linear fit of the logarithmic power against distance leads only to a somewhat objective estimate of attenuation: Q appears to be near 45. It should perhaps also be mentioned that the peak frequency appears to decrease slightly away from the lake, as one would expect from consideration of attenuation, but the effect is so small that not much significance can be attached to it.

The generation of these high frequency surface waves is not understood: if they are generated on the lakeshore by impounding waves, we would not expect the relatively well-defined linear wavefronts observed. If the

high power near the west end can be considered to be anomalous, the waves could be ascribed to a resonant effect due to wave action in the lake: then their frequency should be predictable from theoretical considerations such as given by Longuet-Higgins (1950). In their Figure 2, they give the lowest resonance peak for $2\pi fh/\beta = 1$, with β the shear velocity, and h the depth of the sea. For 1 Hz waves and a representative shear wave velocity (3.3 km/s), we require a lake depth on the order of 500 m, while the actual maximum depths are only about 100 m. Thus, we must assume that the 1 Hz wave is perhaps the resonant frequency of the low-velocity surface layer, suggested by Clee, Barr and Berry and others. Using the alternative resonance estimate, $T = 4h/\beta$, leads to $h \approx 700$ m.

Another noteworthy feature in the power spectra are the multiple peaks near 5.5 and 6 Hz. Their power attenuates rapidly away from the Yellowknife area and is barely visible at the west end (R1). Weichert (1973) ascribed these peaks to mining machinery in the city's gold mines. The peak at 4 Hz and other smaller ones that Weichert identified as instrumental have indeed disappeared now.

5. DISCUSSION AND CONCLUSIONS

The Canadian Seismic Array Monitor has now operated continuously for over a year. The detailed statistical evaluation of the 1974 CANSAM detection log and associated studies have led to the following results, conclusions and recommendations.

Despite the start-up problems always expected for a complex system such as CANSAM, operational status of the detector was achieved during about 93% of the possible time. Comparison with the operation of the Canadian Standard Station, YKC, showed that CANSAM reported most teleseismic and good regional

events reported by the standard station. The percentage of missed events reflects the CANSAM downtime, but events are also missed, for instance, due to the limited CANSAM detection pass band. It must be emphasized here, however, that this comparison is not quite partial: although the station operators are instructed to base their visual event reports on the standard station seismograms, it is in fact known that many reported events are picked from standard station records only after seeing them on the array monitor seismogram.

Comparison of automatic event onset times with those reported for the higher amplitude events by the operator-analyst shows a variance of about one second, with the trend of the mean towards earlier automatic readings. This scatter is not inconsistent with that expected from visually reading standard seismograms: thus, if the percentage of CANSAM operational status can be slightly improved, it appears that the standard operation of the YKC short-period station can be terminated. Final decision, however, must await at least one year of more detailed analysis of CANSAM detections and data for Canadian events.

The annual variation of seismic background at YKA has a strong effect on the detection threshold. Two seasons of approximately 6 months each can be very clearly distinguished and correlated with the presence (winter-spring) or absence (summer-fall) of an ice cover on Great Slave Lake. The designation "winter" and "summer" has been adopted simply for its descriptiveness. The actual dates precede the corresponding astronomical seasons by perhaps 2 to 3 weeks and the summer-fall period appears slightly shorter. In 1974 we defined the seismic summer as the period 1 June to 30 November.

Past off-line experiments in continuous beamforming and detection using YKA short-period data have been conducted during winter and spring, not only because of this difference in noise background, but also because during past summers technical operating conditions were strongly affected by lightening strokes and their consequences. Upgrading of the physical array installation over the years has resulted in much improved operation and comparable performance during all seasons.

For winter conditions, the teleseismic detection threshold in the frequency level 1 to 3 Hz as defined by a 50% false alarm ratio has been shown to lie near 10 nm/s, corresponding to m_b4.0 to 4.1, if an average teleseismic attenuation factor of $Q = 3.8$ is assumed. False alarm rates for other threshold settings can be predicted with good confidence from the figures given in the text. This threshold, or alternatively the false alarm rate for a desired magnitude, has been improved during 1974 on-line operation over that obtained during CANSAM test runs on ISM data, probably resulting from the elimination of the noise associated with the intermediate analog tape recording.

Throughout 1974 the detection process was based on the phased sum of the single channel logarithmic signals: the obtained false alarm relation confirms very accurately the earlier evaluation of the log-sum process vis-à-vis the conventional linear phased sum made by Weichert (1975-a), and this confirms the earlier made claim of lower false alarm rates with this non-linear method. As long as raw data are available for post-detection processing, the log-sum process will therefore continue to be used for detection.

The high noise level during the summer has unfortunately proven to be worse than anticipated. The 50% false alarm rate under the 1974 conditions was already reached near m4.6 to 4.8. Peak amplitudes of the summer noise component occur at the lower end of the current detection pass band and show a surprisingly high visual correlation across the array. Visual measurements, as well as power spectrum analysis, suggest that the summer noise is generated on Great Slave Lake and propagates across the array as an approximately 1.2 Hz surface wave. The generation of this wave is not understood, but it is suggested that the frequency of the peak power may be a resonance phenomenon related to the surficial granite layer under YKA.

Effective measures for suppression of this surface wave before the automatic detection process appears difficult. Because it crosses the array as a rather linear front, it passes through the log-sum process with appreciable power. This is in contrast to the local one-second surface waves generated by explosions in the mines within 5 to 15 km from the array, which exhibit a well-defined curvature across the array and therefore are suppressed.

The detection beams formed by the CANSAM extend only to a maximum slowness of 0.14 s/km and this does not include the optimum beam for the lake noise which propagates from about 150° with a velocity of about 3 km/s. The 2.5 km seismometer spacing in the array leads to a Nyquist wave number of 0.2 km^{-1} ; therefore, the surface wave is actually space-aliassed right into the wave number range of teleseismic interest: this precludes wave-number filtering. Because these waves usually consist of several cycles of quite sinusoidal oscillations within the narrow predetection passband, side lobes are well developed and lead to the observed high number of detections on a broad band of teleseismic beams extending east-west with a small northerly slowness component. Unfortunately, this includes all Eurasian beams.

A simple method of decreasing the number of detections on unwanted signals and noise is the inhibition of beams with little or no interest. It is not suggested to omit these beams from the program because an appreciable fraction of their detections would be expected to spill to neighboring beams, but simply to ignore power maxima on them. This would lower the number of detections and allow the detection logic to continue searching for events (maxima) on other beams. In the present detection logic these possible other events would be suppressed while the system is in detection status.

The other obvious but not very attractive solution is a shift of the detection passband towards higher frequencies. The current passband was already selected, not necessarily with a view towards a maximum number of event detections, but with a subjective bias in favour of the higher frequencies of underground nuclear explosions. Eurasian explosions observed at YKA have appreciable power up to about 5 Hz. Although during winter conditions it is believed that the maximum signal-to-noise ratio of the phased beam is between 1 and 2 Hz, during summer the maximum may well lie considerably higher. This must be investigated and, if advisable, the lower skirt of the detection passband redesigned to at least match the slope of the 1 Hz noise peak. Provisionally, a corner of 2.5 Hz to 3 Hz and a slope of 12 to 18 db/octave appear desirable. The upper corner frequency should, of course, remain below the 5.5 Hz cultural noise peak. Additional considerations are the qualitatively known decrease in signal coherence at the higher frequencies, and the narrowing of the beam response. Beam spacing would very clearly have to be decreased below the current 0.02 s/km.

The effect of the proposed changes on the usefulness of YKA for studies of Canadian seismicity is uncertain. Near-regional P phases have relatively high frequencies and should not be severely suppressed. Detection of S and L_g phases is currently not near optimum because of their lower frequency and because their velocities allow only sidelobe detections. This is not considered to be a serious problem, since optimization of the short-period YKA for regional events may require a separate parallel processing program in any case, and thus will be dealt with independently.

For the future teleseismic on-line mode, a combination of beam restriction and a different summer detection passband will most likely be

selected. During winter conditions, beam restriction and spacing will have a small effect and results presented in this paper will not be improved dramatically. The amount of effort that will be dedicated towards such changes will largely depend on a critical evaluation of the usefulness and need of CANSAM contribution to international efforts.

REFERENCES

Anglin, F.M. (1971). Detection capabilities of the Yellowknife seismic array and regional seismicity, Bull. Seism. Soc. Am., 61, 993-1008.

Barr, K.G. (1971). Crustal refraction experiment: Yellowknife 1966, J. Geophys. Res. 76, 1929-1947.

Birtill, J.W., and F.E. Whiteway (1965). The application of phased arrays to the analysis of seismic body waves, Phil. Trans. Roy. Soc. Lond. A, 248, 421-493.

Briscoe, H.W., and P.L. Fleck (1965). Data recording and processing for the experimental Large Aperture Seismic Array, Proc. IEEE, 53, 1852-1859.

Burch, R.F. (1969). A comparison of the short period seismic noise at the four UKAEA type arrays and an estimate of their detection capabilities, AWRE Report No. 79/68, Aldermaston.

Capon, J. (1961). On the asymptotic efficiency of locally optimum detectors, IRE Trans. Inf. Theory, 7, 67-71.

Clee, T.E., K.G. Barr, and M.J. Berry (1974). Fine structure of the crust near Yellowknife, Can. J. Earth Sci., 11, 1534-1549.

Green, P.W., E.J. Kelly, and M.J. Levin (1966). A comparison of seismic array processing methods, Geophys. J.R. astr. Soc., 11, 67-84.

Hoffman, P. (1969). Proterozoic paleocurrents and depositional history of the East Arm Fold Belt, Great Slave Lake, N.W.T., Can. J. Earth Sci., 6, 441-462.

Kanasewich, E.R., C.D. Hemmings, and T. Alpaslan (1973). N-th rooth stack non-linear multichannel filter, Geophys. 38, 327-338.

Lacoss, R.T., R.E. Needham, and B.R. Julian (1974). International Seismic Month event list, Lincoln Laboratory, MIT, Technical Note 1974-14.

Longuet-Higgins, M.S. (1950). A theory of the origin of microseisms, Phil. Trans. Roy. Soc., London, 243, A857, 1-35.

Manchee, E.B., and H. Somers (1966). The Yellowknife seismological array, Publ. Dom. Obs., Ottawa, 32, No. 2.

Manchee, E.B., and W.D. Cooper (1968). Operation and maintenance of the Yellowknife seismological array 1966-68, Seism. Ser. Dom. Obs., 1968-2.

Manchee, E.B., and D.H. Weichert (1968). Epicentral uncertainties and detection probabilities from the Yellowknife seismic array data, Bull. Seism. Soc. Am., 58, 1359-1377.

Manchee, E.B., and R.B. Hayman (1972). The radio telemetry installation at the Yellowknife seismic array, Publ. Earth Phys. Br., EMR, Ottawa, 43, No. 9.

Melton, B.S., and P.R. Karr (1957). Polarity coincidence scheme for revealing signal coherence, Geophys. 22, 553-564.

Muirhead, K.J. (1968). Eliminating false alarms when detecting seismic events automatically, Nature, 217, 533-534.

Weichert, D.H., E.B. Manchee, and K. Whitham (1967). Digital experiments at twice real-time speed on the capabilities of the Yellowknife seismic array, Geophys. J.R. astr. Soc., 13, 277-295.

Weichert, D.H., and K. Whitham (1969). Geophysical results from digital processing of Yellowknife array signals, Publ. du Bureau Central Seism. Int., Ser. A, Trav. Scient., 24, 29-43.

Weichert, D.H., and E.B. Manchee (1969). A photogrammetric resurvey of the Yellowknife seismic array, Seismol. Ser. Dom. Obs., 1969-2.

Weichert, D.H. (1973). An attempt to detect gravitational waves with the Yellowknife seismic array, Geophys. J.R. astr. Soc., 35, 337-342.

Weichert, D.H. (1975-a). Logarithmic beam forming for suppression of false alarms in seismic detection, Geophys. Res. Lett., 2, No. 4, p. 121.

Weichert, D.H. (1975-b). The role of medium aperture arrays: The Yellowknife system, in: Exploitation of Seismograph Networks, NATO Adv. Study Inst. Ser. E., 11, 167-195.

FIGURES

FIGURES (cont'd)

TABLES

TABLE I Beam arrangement for YKA-CANSAM processing system. The octal beam code is listed, followed by the beam azimuth (nearest degree) and dT/dΔ (ms/km)

N-S Component		E-W Slowness Component										
		-100	-80	-60	-40	-20	0	20	40	60	80	100
	No.	156	157	160	161	162	163	164	165	166	167	170
100	Az.	315	321	329	338	349	0	11	22	31	39	45
	dT/dΔ	141	128	117	108	102	100	102	108	117	128	141
		143	144	145	146	147	150	151	152	153	154	155
80		309	315	323	333	346	0	14	27	37	45	51
		128	113	100	89	82	80	82	89	100	113	128
		130	131	132	133	134	135	136	137	140	141	142
60		301	307	315	326	342	0	18	34	45	53	59
		117	100	85	72	63	60	63	72	85	100	117
		115	116	117	120	121	122	123	124	125	126	127
40		292	297	304	315	333	0	27	45	56	63	68
		108	89	72	57	45	40	45	57	72	89	108
		102	103	104	105	106	107	110	111	112	113	114
20		281	284	288	297	315	0	45	63	72	76	79
		102	82	63	45	28	20	28	45	63	82	102
		67	70	71	72	73	74	75	76	77	100	101
0		270	270	270	270	270	--	90	90	90	90	90
		100	80	60	40	20	0	20	40	60	80	100
		54	55	56	57	60	61	62	63	64	65	66
-20		259	256	252	243	225	180	135	117	108	104	101
		102	82	63	45	28	20	28	45	63	82	102
		41	42	43	44	45	46	47	50	51	52	53
-40		248	243	236	225	207	180	153	135	124	117	112
		108	89	72	57	45	40	45	57	72	89	108
		26	27	30	31	32	33	34	35	36	37	40
-60		239	233	225	214	198	180	162	146	135	127	121
		117	100	85	72	63	60	63	72	85	100	117
		13	14	15	16	17	20	21	22	23	24	25
-80		231	225	217	207	194	180	166	153	143	135	129
		128	113	100	89	82	80	82	89	100	113	128
		0	1	2	3	4	5	6	7	10	11	12
-100		225	219	211	202	191	180	169	158	149	141	135
		141	128	117	108	102	100	102	108	117	128	141

TABLE II Time losses of CANSAM system in 1974

Power failures or power variation	7500 minutes
Disk problems	5600
Program changes and operator training	4500
Digital tape unit, repair of	2300
Inverter problems	1500
Maintenance	1000
Total identified	22400
Not identified, probably mostly power problems	14600
Total loss	37000 minutes
out of	470000 (7.9%)

TABLE III Comparison of presumed teleseisms reported by YKC standard station operator and automatic CANSAM bulletin.

Month	No. of YKC phase reports	No. of Cansam-missed detections due to being inoperational	Other causes
February	186	19	12
March	205	3	11
April	179	32	3
May	194	40	3
June	138	10	0
July	106	4	3
August	123	12	3
September	53	0	1
October	66	1	2
November	91	5	2
December	197	17	3
TOTAL	1538	143 (9.3%) exclusive Feb. & March	43 (2.8%) (1.7%)

TABLE IV Comparison of YKC operator-reported regional events AND automatic CANSAM detections

Month	No. of YKC regionals	CANSAM not Operational	CANSAM Detected	"High Quality" Regionals and CANSAM Operational	CANSAM Dectected of Last Column
April	96	15	60	21	19
May	67	11	46	23	22
June	27	0	17	17	15
July	22	0	13	9	9
August	17	1	14	10	10
September	27	0	16	8	6
October	21	0	15	7	7
November	29	0	22	10	9
December	58	3	42	10	10
	364	8.2%	67.3%	115	93%

TABLE V Summer-noise detections selected for time-domain analysis

Date	Time	Beam	Log A/T	Background	Least squares azimuth	Least squares slowness
74 Jun 23	0713	114	10050	3950	146	364 ms/km
74 Jul 2	1000	113	11050	4650	154	332
74 Jul 29	1846	76	10060	4340	144	398
74 Aug 11	1213	71	11850	5110	145	338
74 Sep 6	0329	102	10220	4880	145	320
74 Oct 11	0901	104	11870	4970	148	301
74 Oct 26	0133	47	11350	4730	155	331
74 Nov 10	0830	65	10970	4460	156	316
74 Nov 19	1747	77	8276	3410	158	333
				Average	150.1	336.9 ms/km

TABLE VI Dates and starting times of 12.8s noise samples selected for spectral analysis

1974 April 8	00 12 Z	37.2 sec	1974 October 22	15 37 Z	44.9 sec
	00 19	18.6		15 50	37.4
	00 21	00.6		15 59	12.6
	01 38	05.7		16 04	26.3
	02 59	19.8		16 08	32.6
	03 13	24.1		16 11	10.1
	03 26	51.1		16 14	48.6
	05 27	38.4		16 25	36.3
	07 28	11.8		16 32	19.8
	09 12	15.7		16 40	00.9

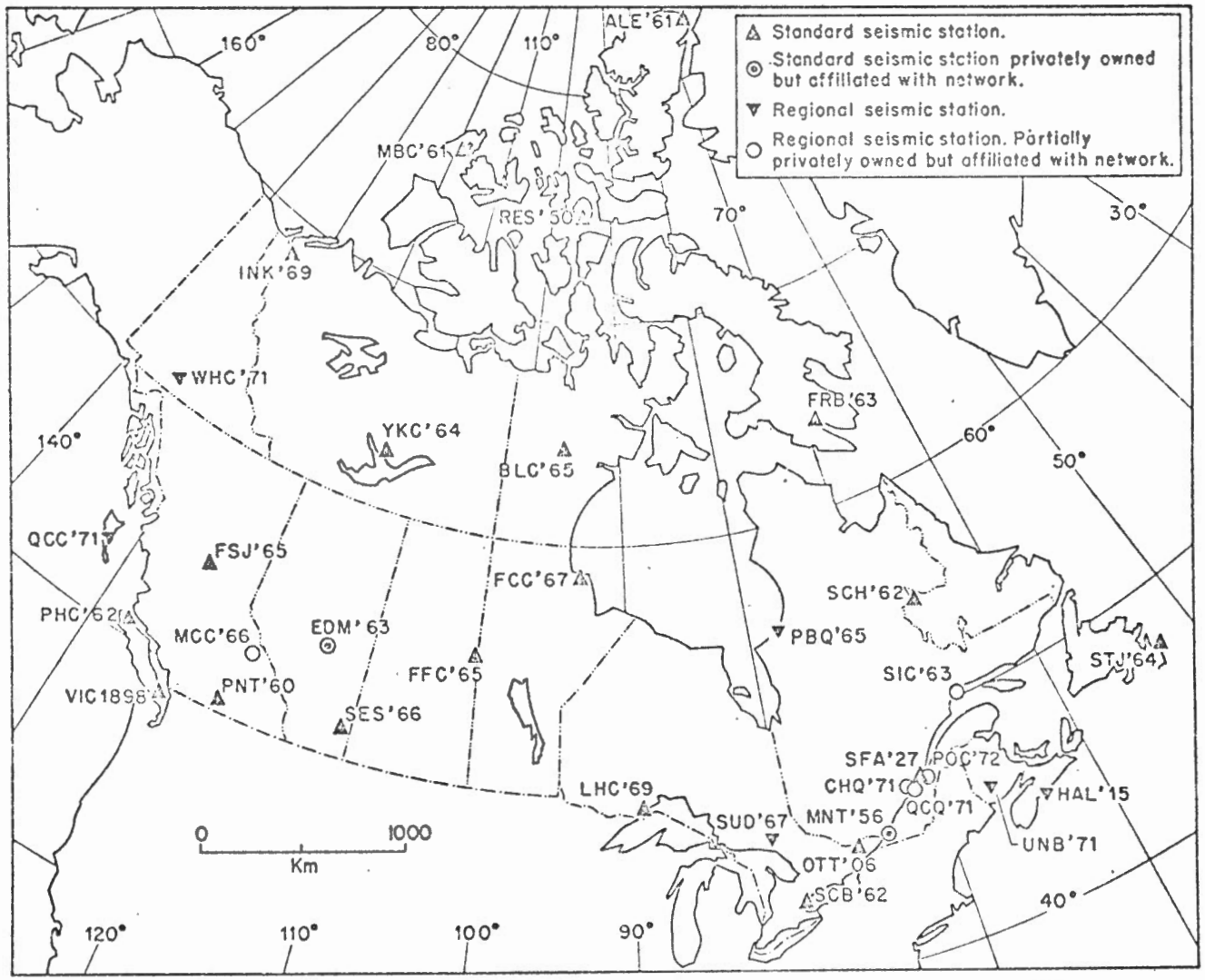

CANADIAN STANDARD AND REGIONAL SEISMOGRAPH STATIONS 1974

FIG 1

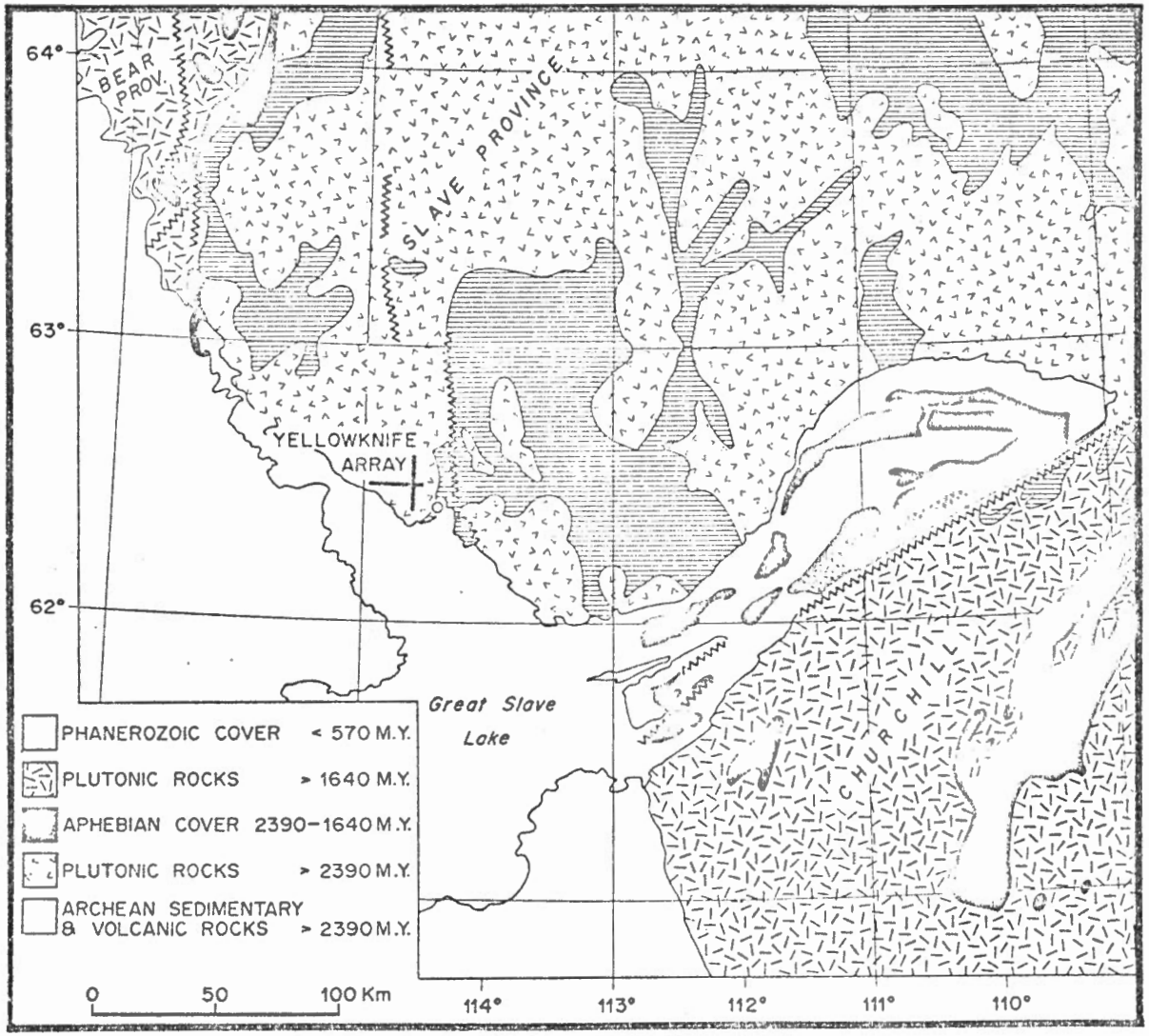
64°
63°
62°
BEAR PROV.
SLAVE PROVINCE
YELLOWKNIFE ARRAY
Great Slave Lake
CHURCHILL
PHANEROZOIC COVER < 570 M.Y.
PLUTONIC ROCKS > 1640 M.Y.
APHEBIAN COVER 2390–1640 M.Y.
PLUTONIC ROCKS > 2390 M.Y.
ARCHEAN SEDIMENTARY & VOLCANIC ROCKS > 2390 M.Y.
0 50 100 Km
114°
113°
112°
111°
110°

FIG 2

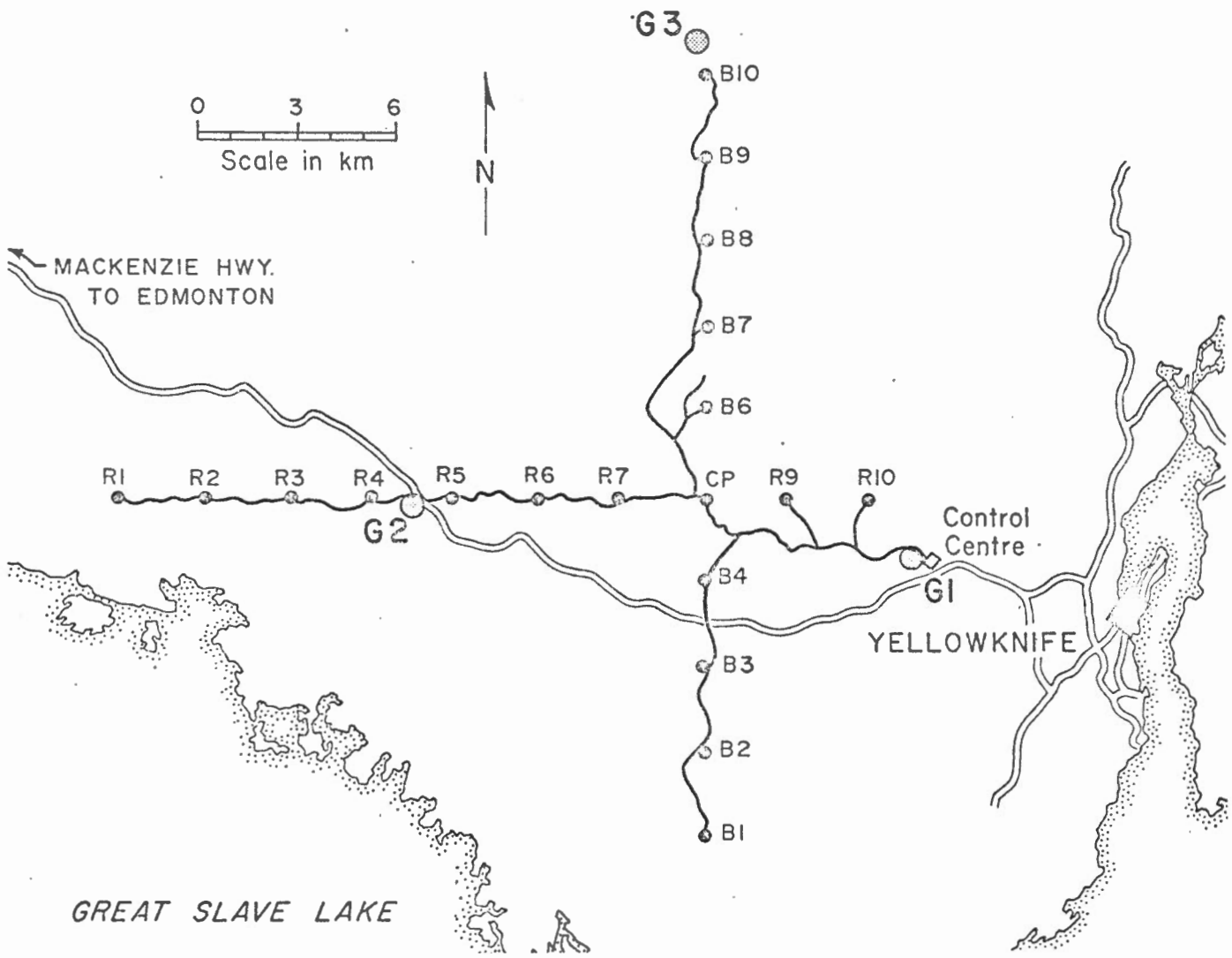
G3
B10
B9
B8
B7
B6
0 3 6
Scale in km
N
MACKENZIE HWY.
TO EDMONTON
R1
R2
R3
R4
R5
R6
R7
CP
R9
R10
G2
Control
Centre
G1
B4
YELLOWKNIFE
B3
B2
B1
GREAT SLAVE LAKE

Fig 3

CANADIAN SEISMIC ARRAY MONITOR, 1974

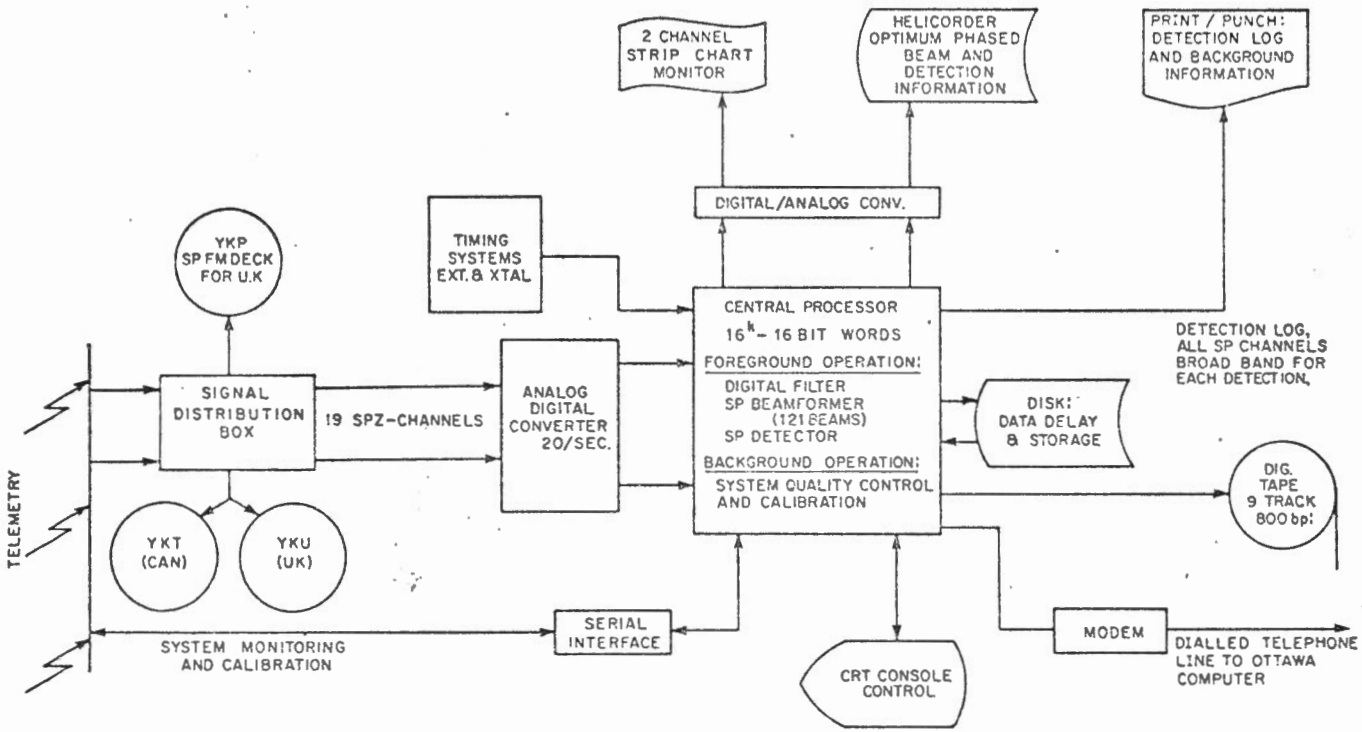

FIG 4

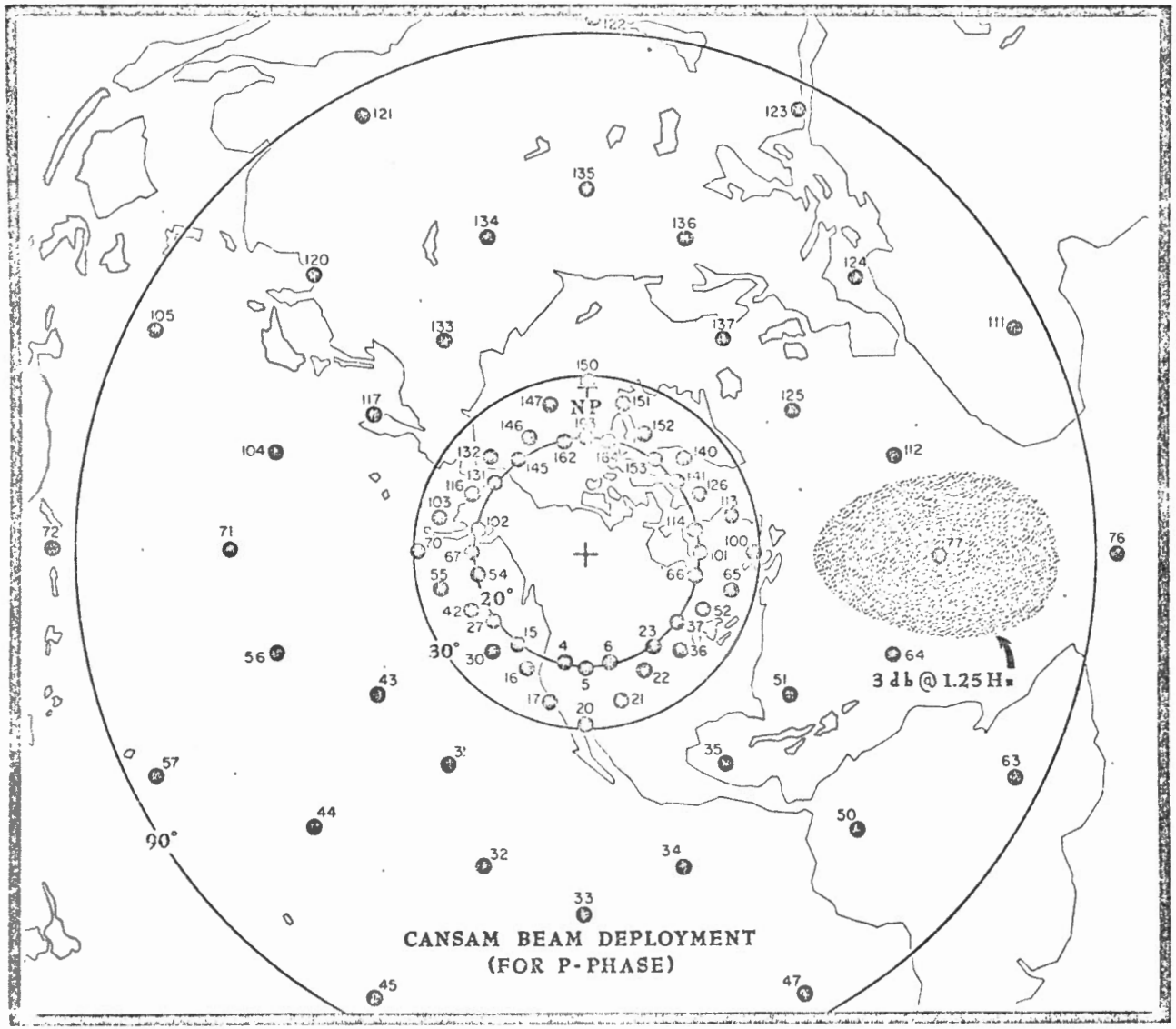

CANSAM BEAM DEPLOYMENT
(FOR P-PHASE)

FIG 5

DOMINANT SIGNAL FREQUENCIES OF SMALL SEISMIC EVENTS ($<m_b$ 4.7) MEASURED AT YKA DURING ISM

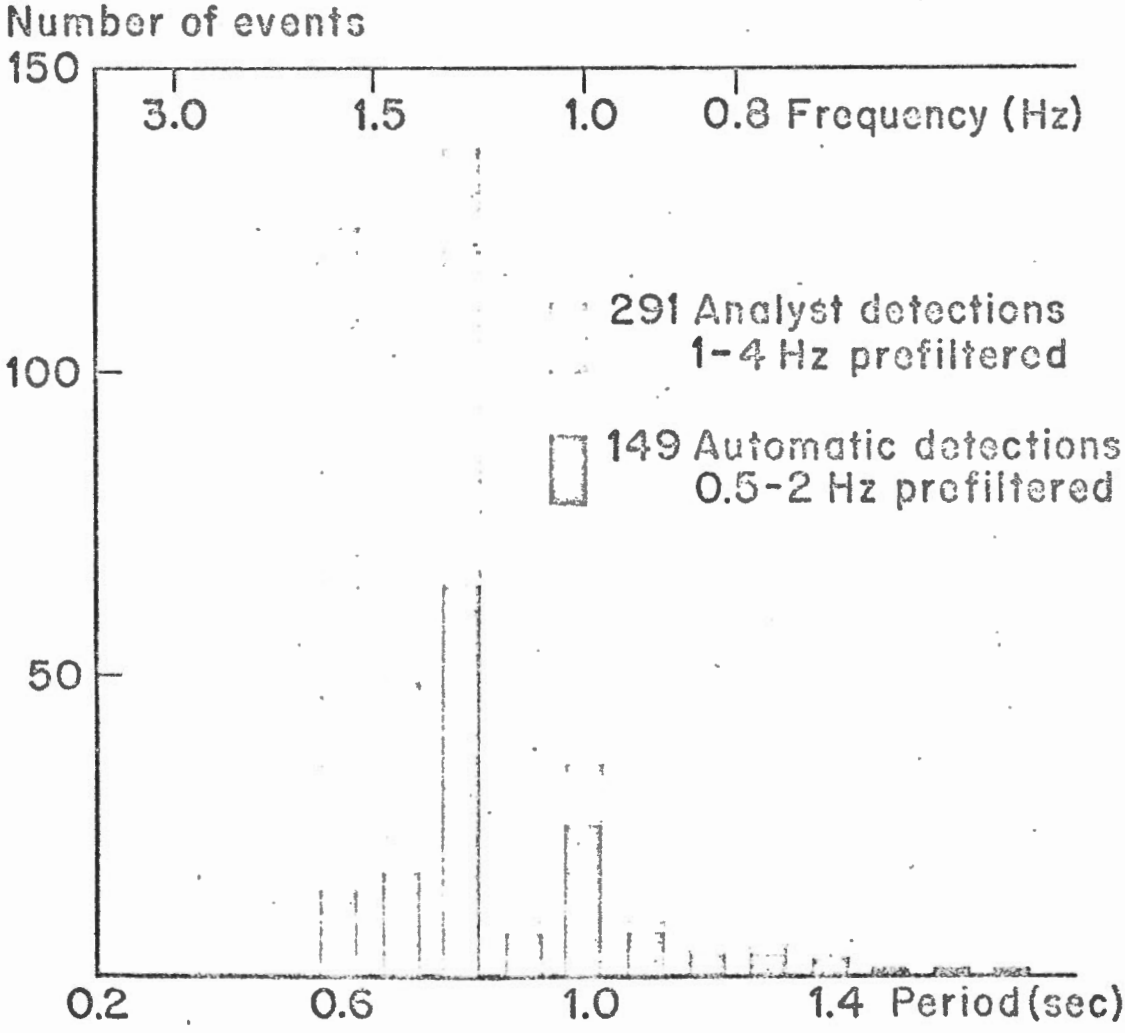

FIG 6

FIG 6

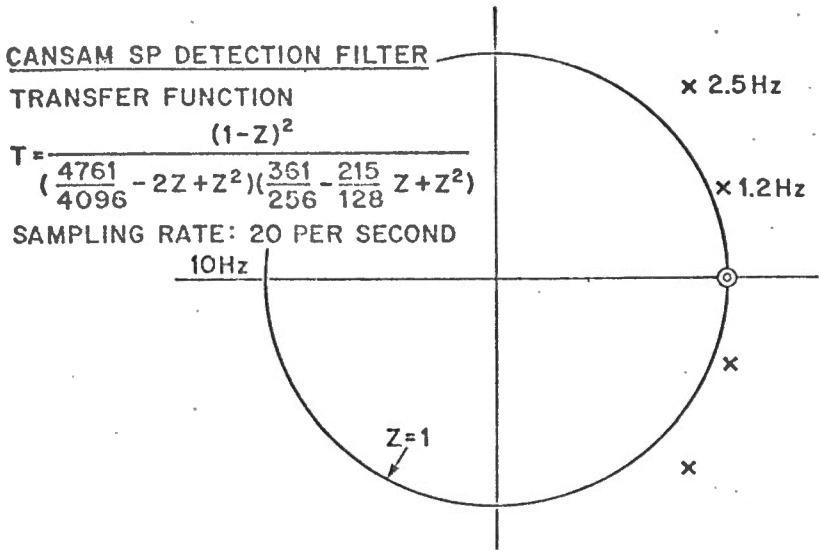
CANSAM SP DETECTION FILTER
TRANSFER FUNCTION
$T = \frac{(1-Z)^2}{(\frac{4761}{4096} - 2Z + Z^2)(\frac{361}{256} - \frac{215}{128} Z + Z^2)}$
SAMPLING RATE: 20 PER SECOND
10Hz
× 2.5Hz
× 1.2Hz
Z=1

a

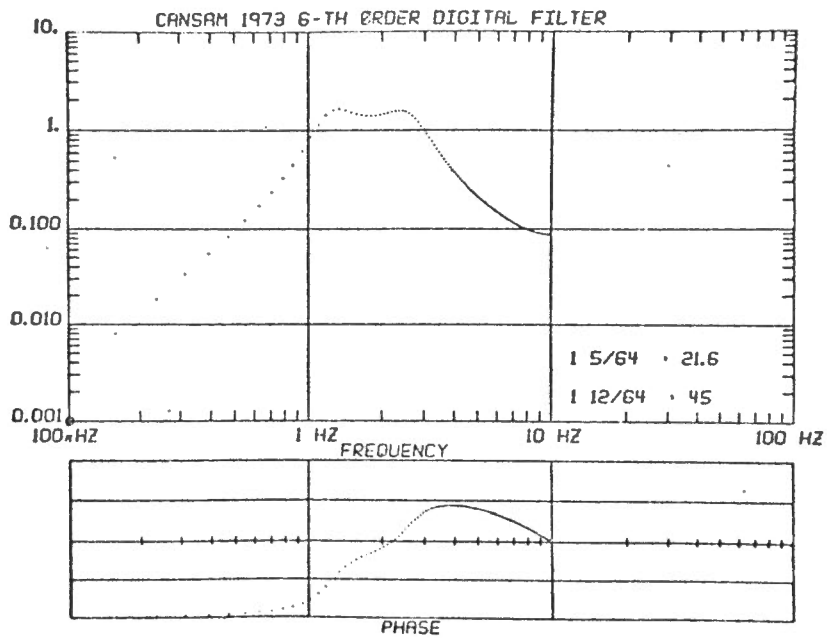
CANSAM 1973 6-TH ORDER DIGITAL FILTER
10.
1.
0.100
0.010
0.001
100 HZ
1 HZ
10 HZ
100 HZ
FREQUENCY
1 5/64 · 21.6
1 12/64 · 45
PHASE

b

FIG 7

FIG 7

DAY 82
23 MARCH 74

YDDDHHMM	SST	BNO	LGA/T	NOISE
40821540	125	111	18289	03054
40821556	461	057	07285	03183
40821619	037	111	07171	02771
40821639	509	122	08459	02975
40821819	069	105	06494	02860
40821859	005	075	17618	02686
40821911	541	003	07527	03019
40821913	198	016	10972	02788
40821914	230	016	21172	03070
40821915	110	003	08377	03023
40821930	573	117	08486	03495
40822039	037	050	07330	02890
40822039	510	057	11445	02797
40822043	085	035	16472	02955
40822044	150	047	13987	03439
40822104	589	057	06328	02740
40822109	125	056	07697	03136
40822159	357	057	17485	02857
40822200	350	057	09839	03512

FIG 8

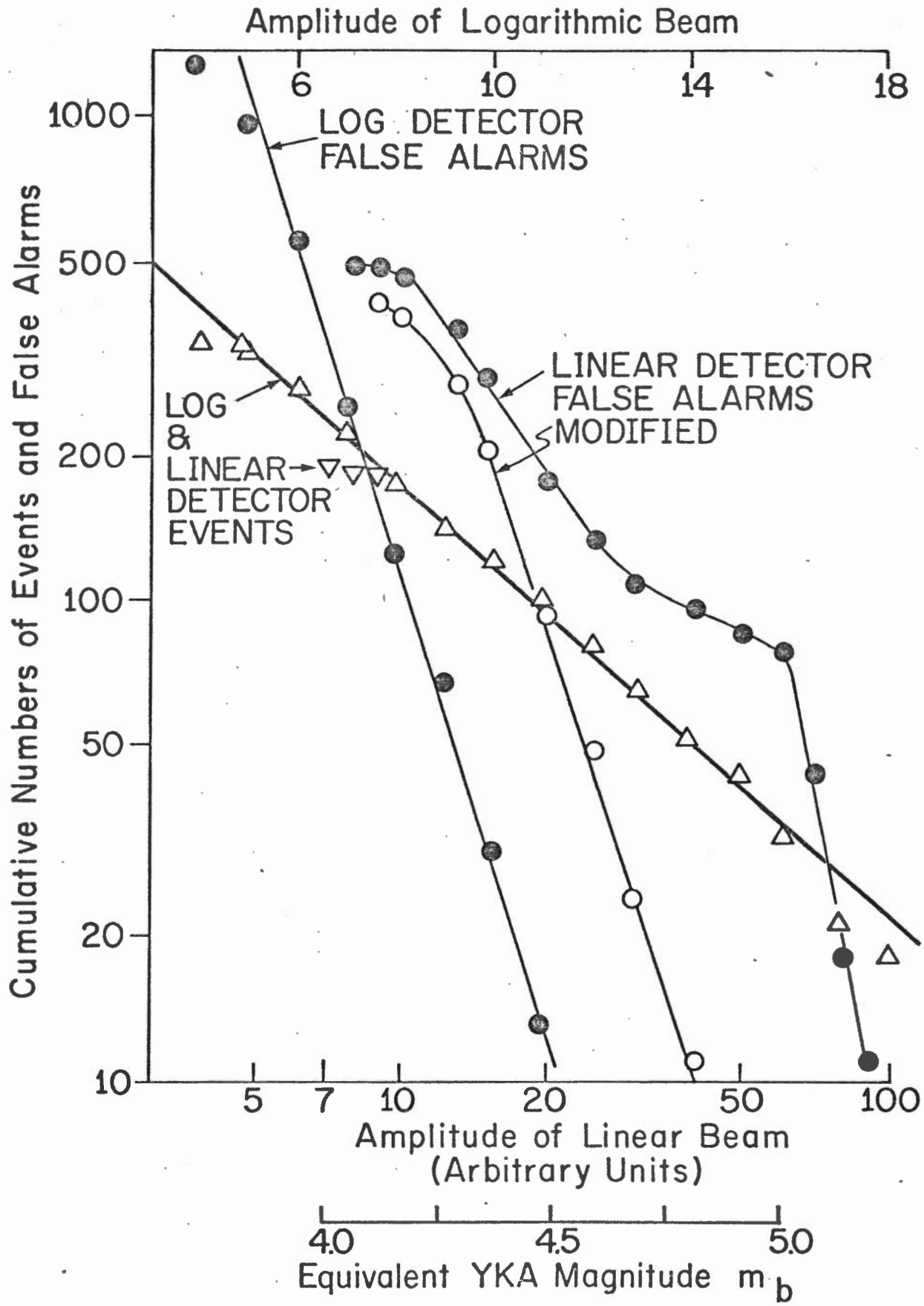
Amplitude of Logarithmic Beam
6
10
14
18
1000
500
200
100
50
20
10
Cumulative Numbers of Events and False Alarms
LOG DETECTOR
FALSE ALARMS
LINEAR DETECTOR
FALSE ALARMS
MODIFIED
LOG
&
LINEAR
DETECTOR
EVENTS
5
7
10
20
50
100
Amplitude of Linear Beam
(Arbitrary Units)
4.0
4.5
5.0
Equivalent YKA Magnitude m_b

FIG. 9.

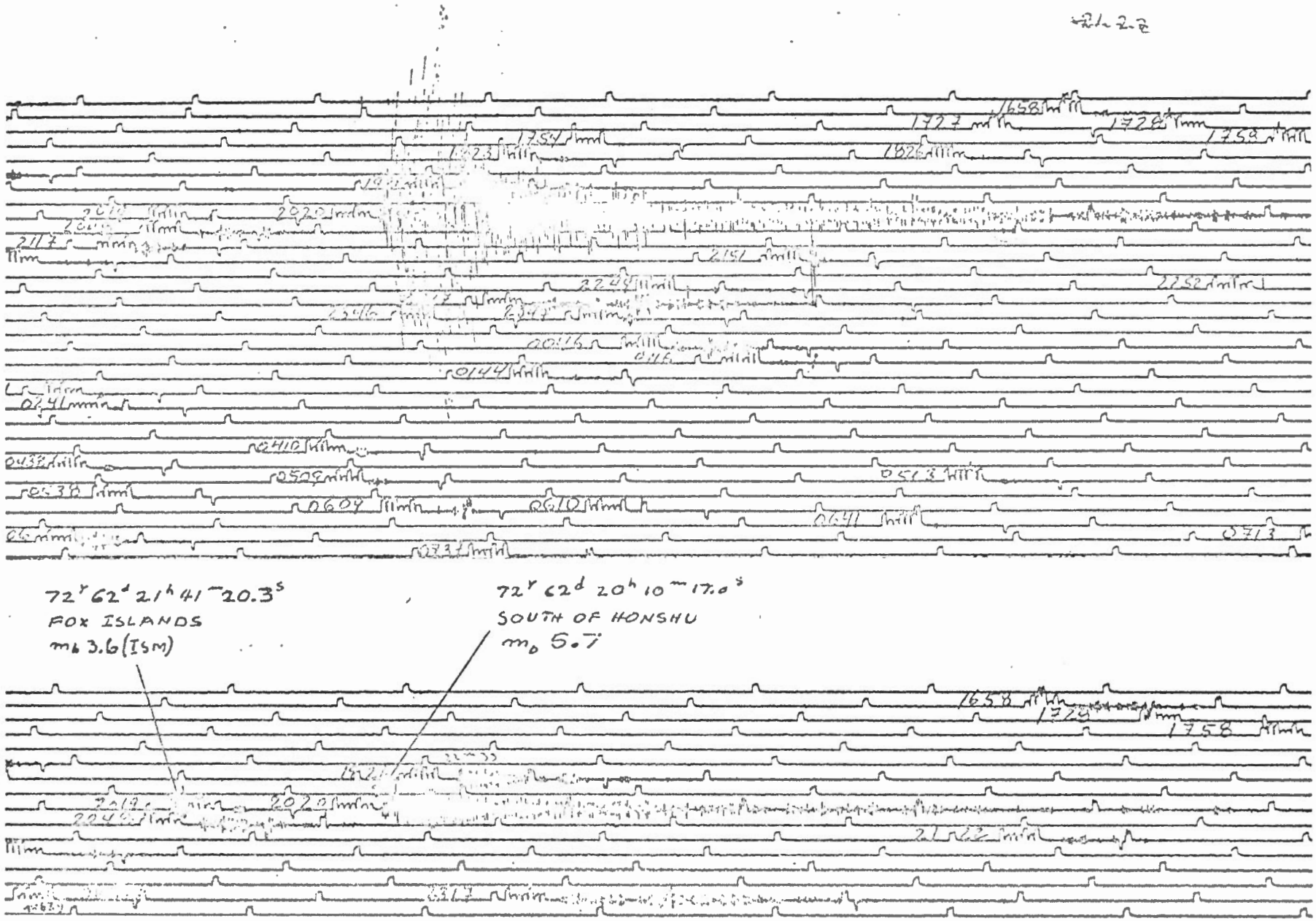
72° 62° 21h 41m 20.3s
FOX ISLANDS
mb 3.6 (ISM)
72° 62° 20h 10m 17.0s
SOUTH OF HONSHU
m0 5.7

FIG. 10

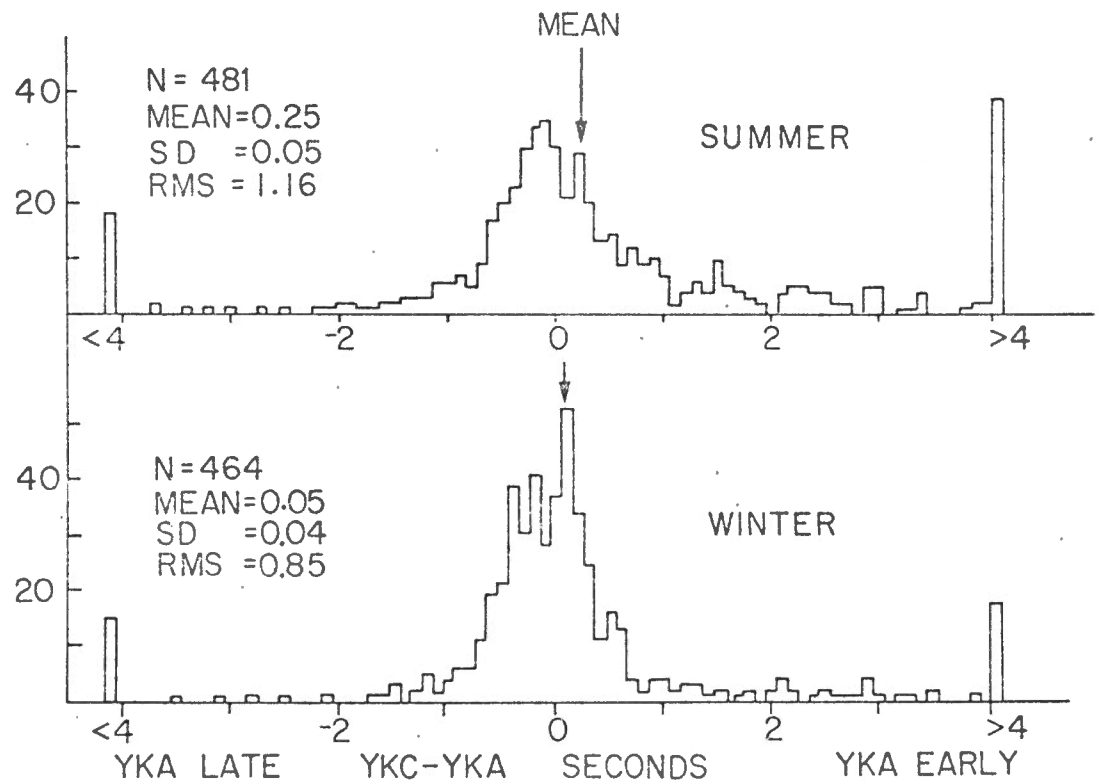
MEAN
N = 481
MEAN=0.25
SD =0.05
RMS = 1.16
SUMMER
40
20
<4
-2
0
2
>4
N=464
MEAN=0.05
SD =0.04
RMS =0.85
WINTER
40
20
<4
-2
0
2
>4
YKA LATE
YKC-YKA
SECONDS
YKA EARLY

FIG 11

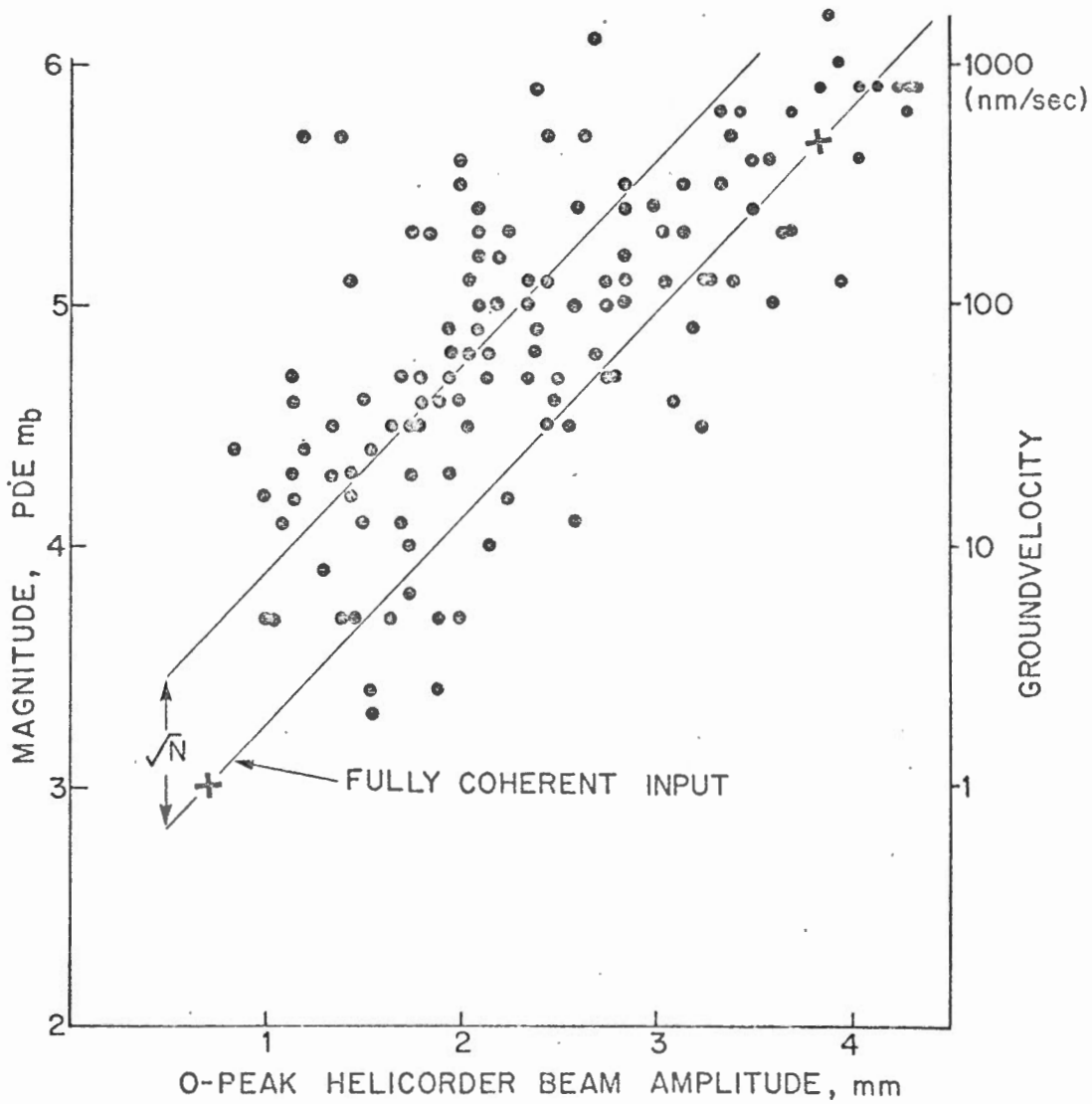
6
5
4
3
2
1
2
3
4
1000
(nm/sec)
100
10
1
MAGNITUDE, PDE mb
GROUNDVELOCITY
√N
FULLY COHERENT INPUT
O-PEAK HELICORDER BEAM AMPLITUDE, mm

FIG 12

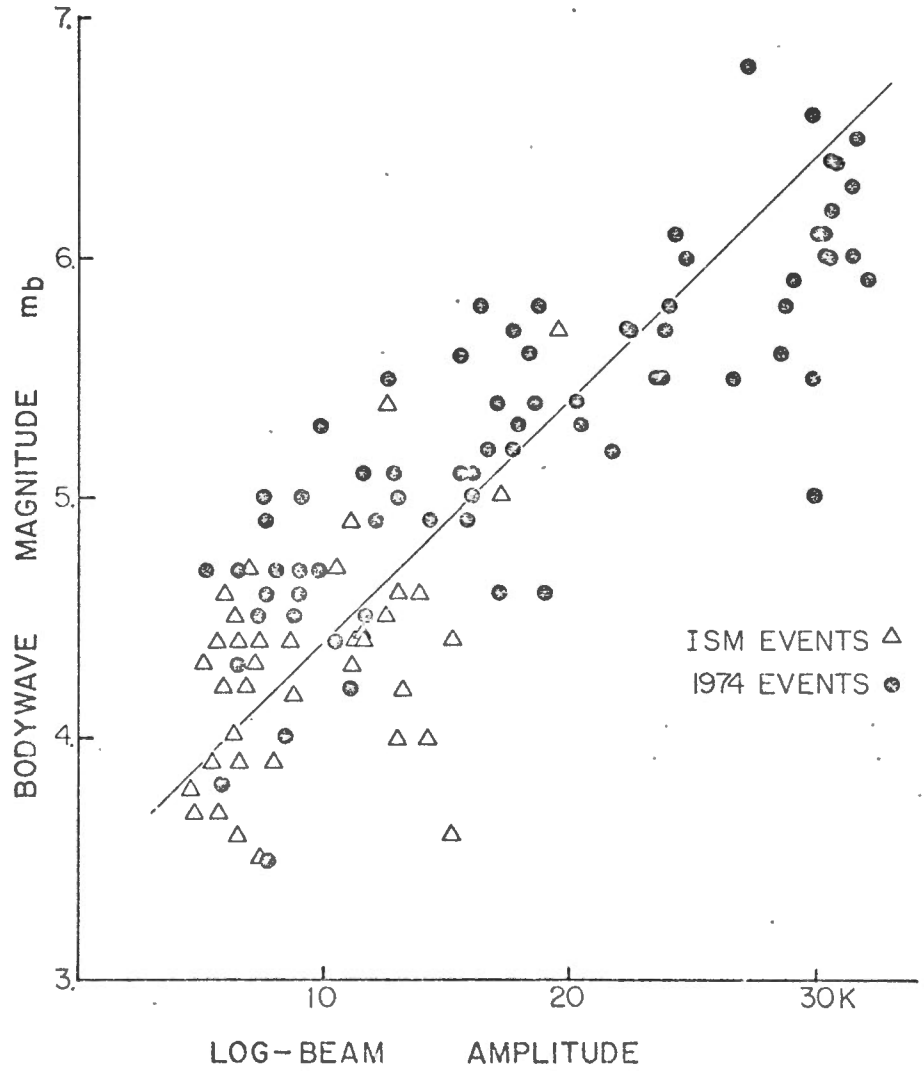
7.
6.
5.
4.
3.
BODYWAVE MAGNITUDE mb
10
20
30K
LOG-BEAM AMPLITUDE
ISM EVENTS △
1974 EVENTS ⊗

FIG 13

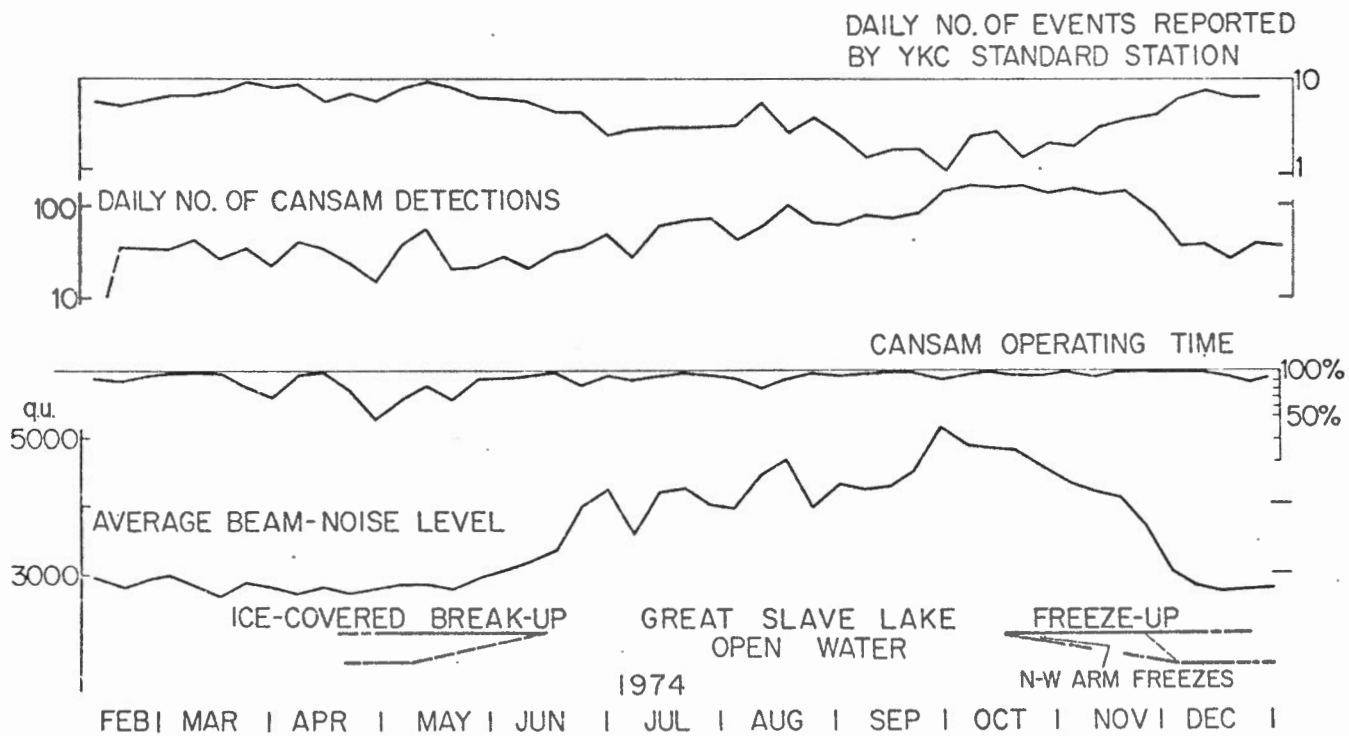
DAILY NO. OF EVENTS REPORTED
BY YKC STANDARD STATION
10
1
100
DAILY NO. OF CANSAM DETECTIONS
10
CANSAM OPERATING TIME
100%
50%
q.u.
5000
AVERAGE BEAM-NOISE LEVEL
3000
ICE-COVERED BREAK-UP
GREAT SLAVE LAKE
OPEN WATER
FREEZE-UP
N-W ARM FREEZES
1974
FEB | MAR | APR | MAY | JUN | JUL | AUG | SEP | OCT | NOV | DEC |

FIG 14

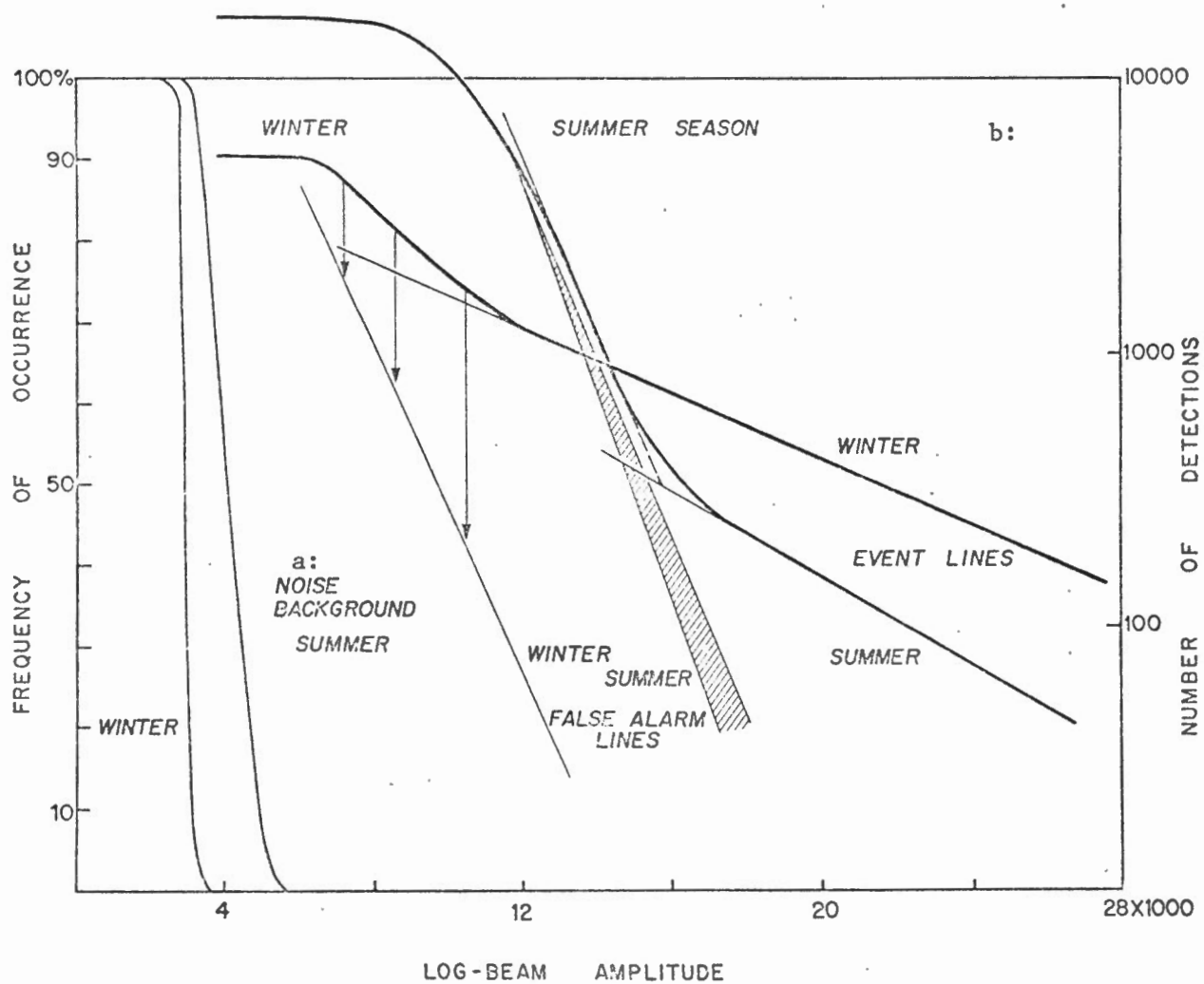
100%
90
50
10
FREQUENCY OF OCCURRENCE
10000
1000
100
NUMBER OF DETECTIONS
WINTER
SUMMER SEASON
b:
WINTER
EVENT LINES
SUMMER
a:
NOISE
BACKGROUND
SUMMER
WINTER
SUMMER
FALSE ALARM
LINES
WINTER
4
12
20
28X1000
LOG-BEAM AMPLITUDE

G 15

7 230674071300E 1.516 NØISE 10 S/SEC
67 NM/S 0.0 0.0 MS/KM

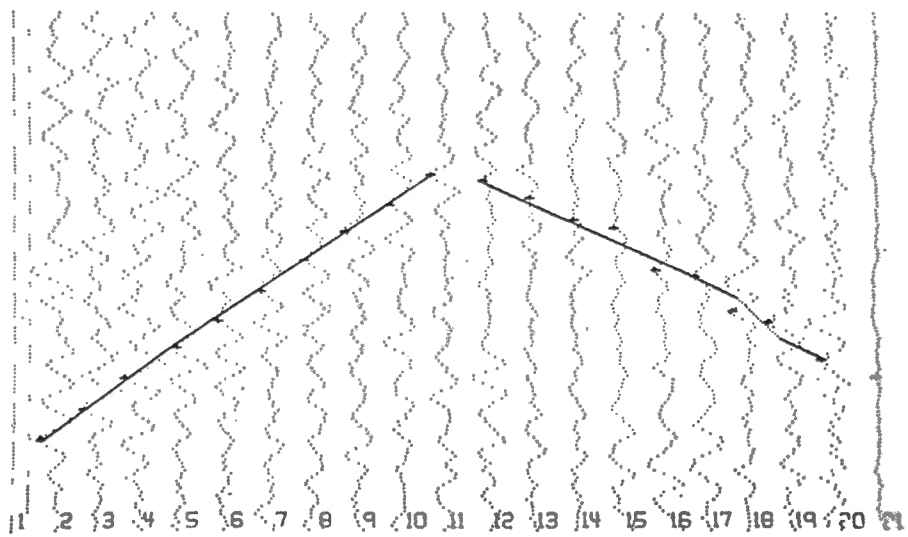

FIG 16 a

0.00 0 TUNED TØ SEISMIC NØISE
7 230674071300E 1.516 NØISE 10 S/SEC
67 NM/S -320.4 209.1 MS/KM

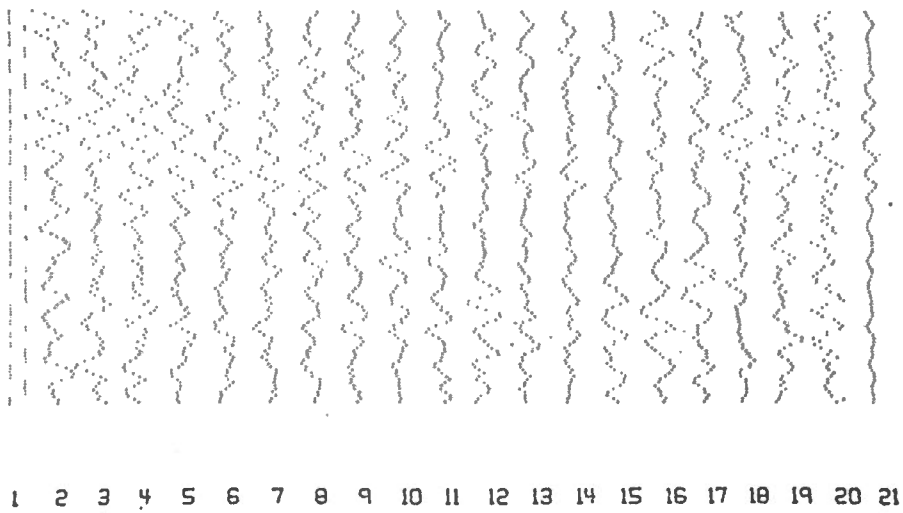

FIG 16 b

0.00 0 AFTER BEAMFØRMING NBR.113
7 230674071300E 1.516 NØISE 10 S/SEC
67 NM/S 80.0 20.0 MS/KM

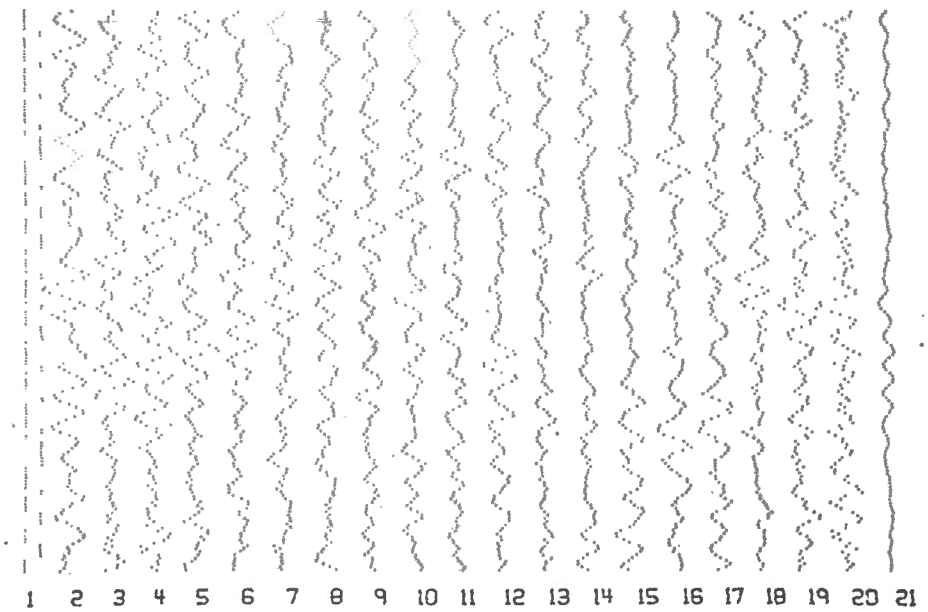

FIG16c

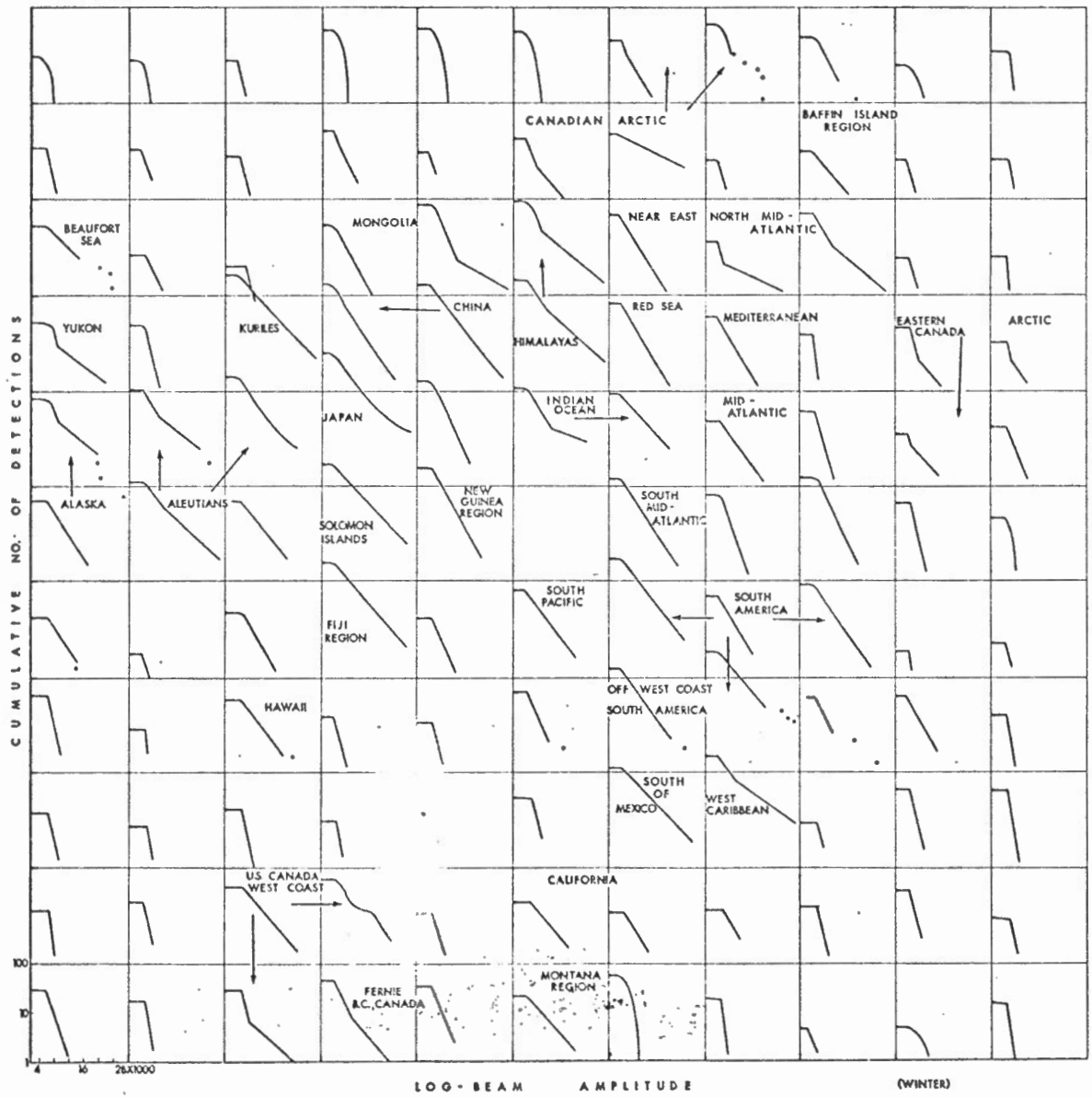

FIG 17a

FIG 17a

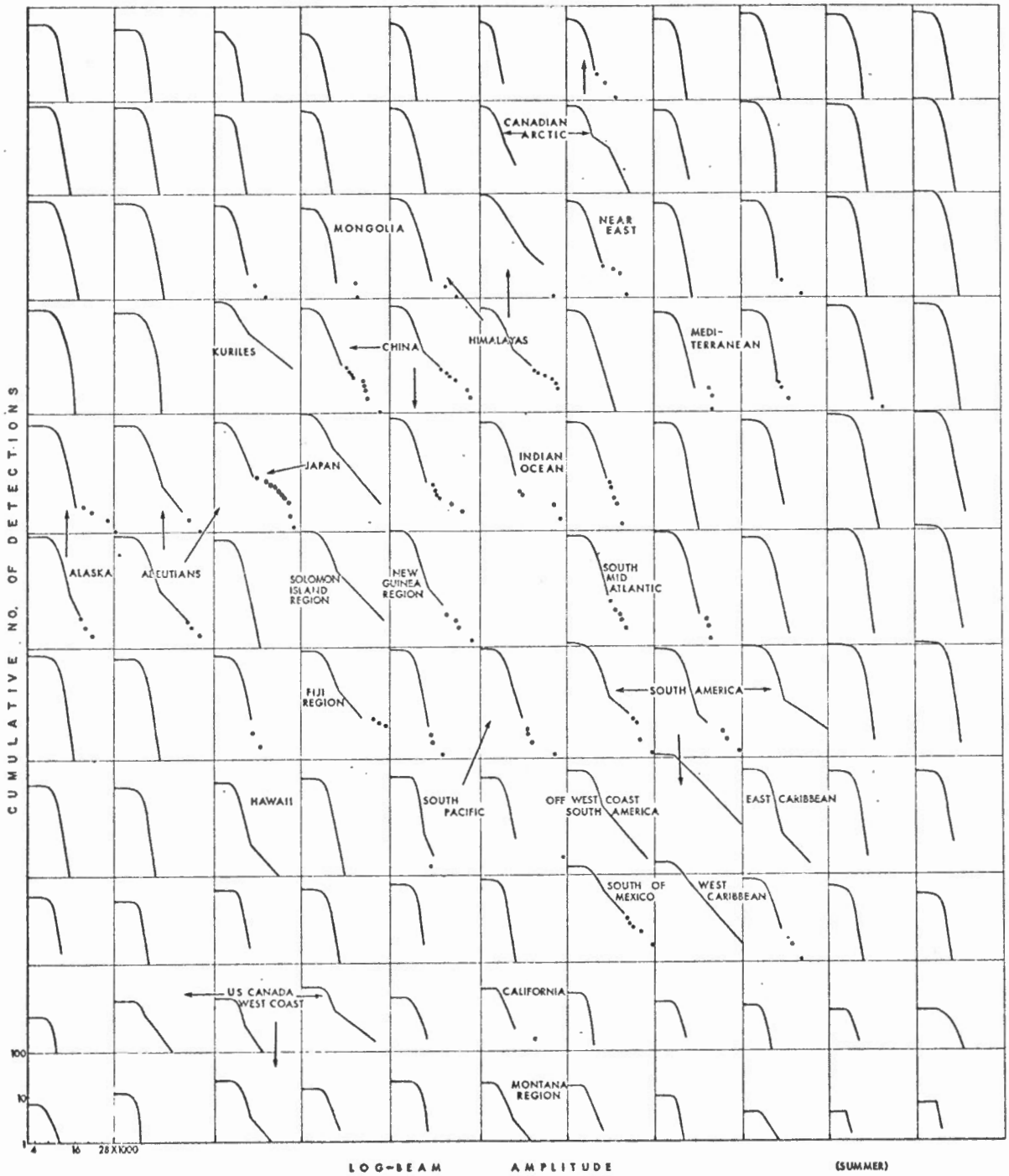

FIG 17.6

FIG 17 b

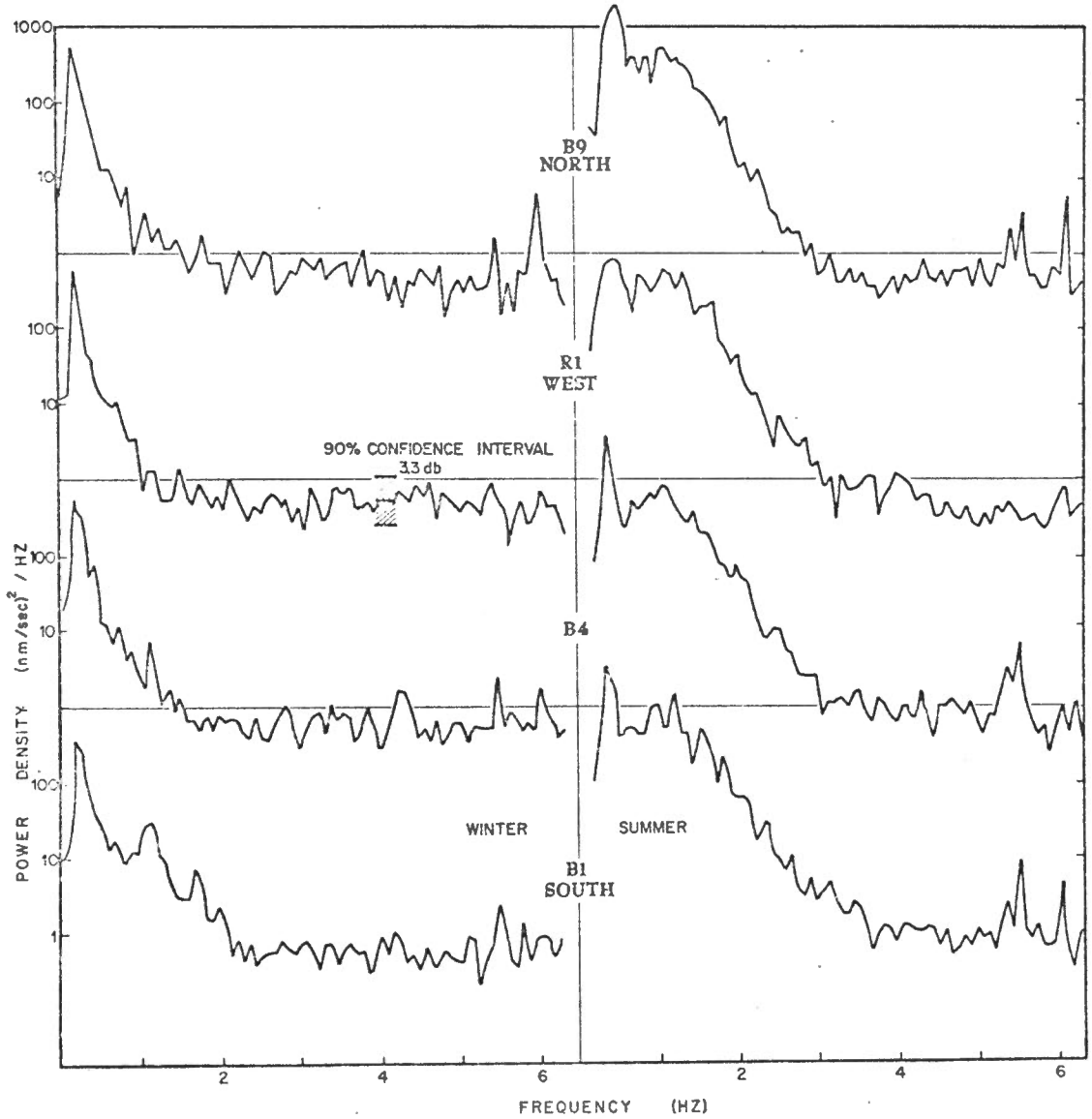
1000
100
10
B9
NORTH
100
10
R1
WEST
90% CONFIDENCE INTERVAL
3.3 db
100
10
B4
100
10
1
B1
SOUTH
WINTER
SUMMER
POWER DENSITY (nm/sec)² / HZ
2
4
6
2
4
6
FREQUENCY (HZ)

a b

FIG 18

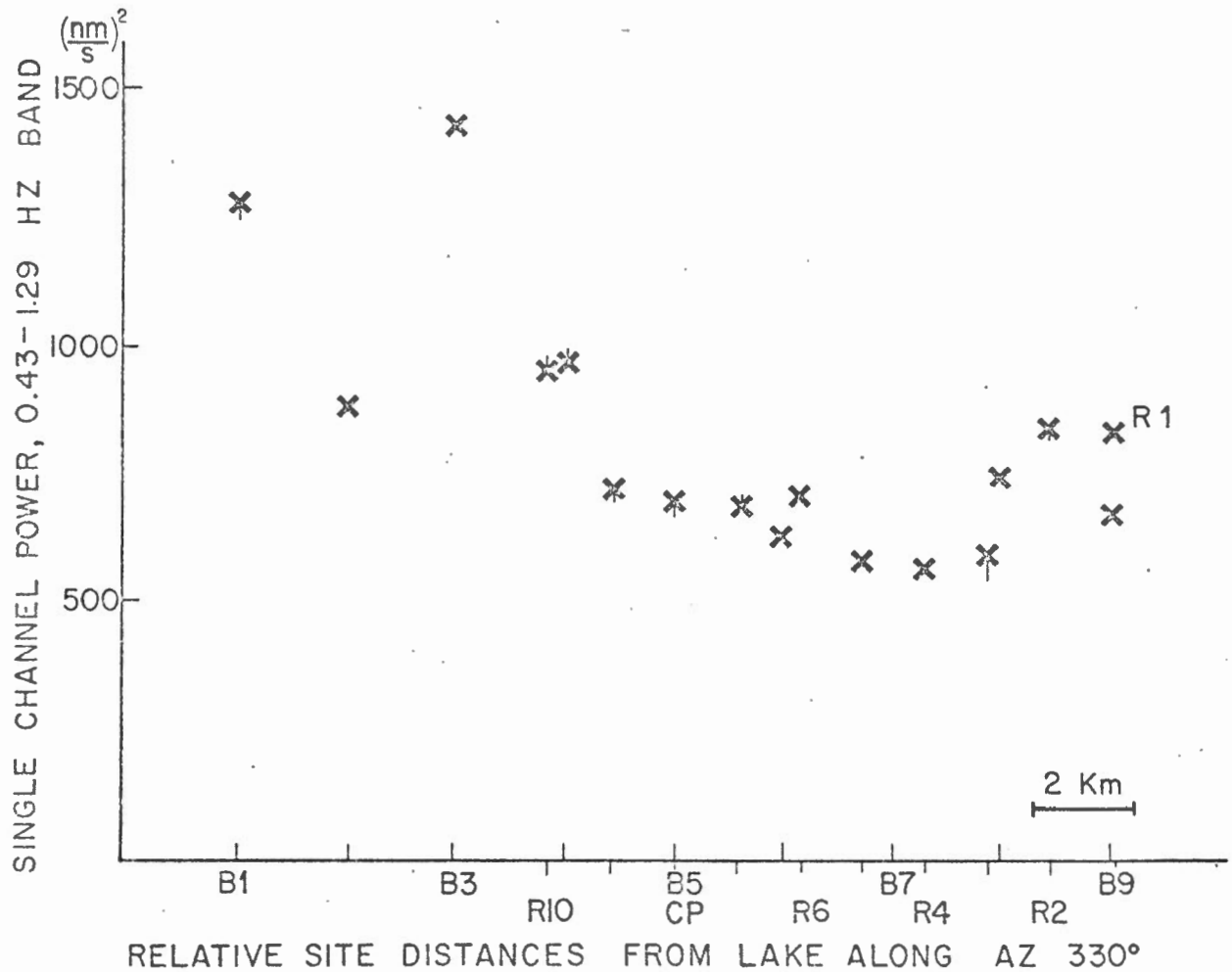
SINGLE CHANNEL POWER, 0.43-1.29 HZ BAND
(nm/s)²
1500
1000
500
R1
2 Km
B1
B3
R10
B5
CP
R6
B7
R4
R2
B9
RELATIVE SITE DISTANCES FROM LAKE ALONG AZ 330°

FIG 19